Voltage-Dependent C-Type Inactivation in a Constitutively Open K$^+$ Channel

Gianina Panaghie,*[†] Kerry Purtell,* Kwok-Keung Tai,[‡] and Geoffrey W. Abbott*[†]

*Greenberg Division of Cardiology, Department of Medicine, and [†]Department of Pharmacology, Cornell University, Weill Medical College, New York, New York; and [‡]The Parkinson's and Movement Disorder Research Laboratory, Long Beach Memorial Medical Center, Long Beach, California

ABSTRACT   Most voltage-gated potassium (Kv) channels undergo C-type inactivation during sustained depolarization. The voltage dependence and other mechanistic aspects of this process are debated, and difficult to elucidate because of concomitant voltage-dependent activation. Here, we demonstrate that MinK-KCNQ1 (I$_{Ks}$) channels with an S6-domain mutation, F340W in KCNQ1, exhibit constitutive activation but voltage-dependent C-type inactivation. F340W-I$_{Ks}$ inactivation was sensitive to extracellular cation concentration and species, and it altered ion selectivity, suggestive of pore constriction. The rate and extent of F340W-I$_{Ks}$ inactivation and recovery from inactivation were voltage-dependent with physiologic intracellular ion concentrations, and in the absence or presence of external K$^+$, with an estimated gating charge, z_i, of ~1. Finally, double-mutant channels with a single S4 charge neutralization (R231A,F340W-I$_{Ks}$) exhibited constitutive C-type inactivation. The results suggest that F340W-I$_{Ks}$ channels exhibit voltage-dependent C-type inactivation involving S4, without the necessity for voltage-dependent opening, allosteric coupling to voltage-dependent S6 transitions occurring during channel opening, or voltage-dependent changes in ion occupancy. The data also identify F340 as a critical hub for KCNQ1 gating processes and their modulation by MinK, and present a unique system for further mechanistic studies of the role of coupling of C-type inactivation to S4 movement, without contamination from voltage-dependent activation.

INTRODUCTION

Voltage-gated potassium (Kv) channels open in response to cellular depolarization to permit K$^+$ ion efflux, facilitating cellular repolarization. Most Kv channels also undergo inactivation, resulting in current decay during sustained depolarization (1,2). This process endows excitable cells with a memory of past action potentials because channels can accumulate in the inactivated state during rapid, sustained firing, eventually leading to interruption of the train of action potentials (3). At slower firing rates, inactivation causes a refractory period between action potentials as channels recover from inactivation upon membrane repolarization, causing after-hyperpolarizations (4). Thus, Kv channel inactivation is an essential determinant of the firing properties of excitable cells (5–7).

In some Kv channels, inactivation is mediated by an N-terminal, cytoplasmic inactivation domain that causes rapid N-type inactivation upon depolarization by binding to the intracellular cavity of the channel and occluding the ion conduction pathway (8–10). In others—and in N-type channels with the inactivation domain removed—distinct, slower inactivation processes are apparent, described variously depending upon several functional features as P-type, U-type, or most commonly C-type. These slow inactivation processes are all thought to involve structural rearrangements in the selectivity filter or nearby residues, in some cases conceptualized as a collapse or constriction of the pore (11,12). Whether this constriction represents a general narrowing of the pore or a simple shift in one or more side chains to disfavor coordination of larger ions is as yet unclear. C-type inactivation is characterized by onset without delay upon depolarization and by sensitivity to external K$^+$ ion concentration, with inactivation becoming slower and less extensive at higher K$^+$ concentrations. Conversely, replacement of external K$^+$ ion with an equal concentration of less permeant ions such as Na$^+$ increases C-type inactivation in *Shaker* and similar slow inactivation processes in other Kv channels such as Kv1.5 (8,13). Extracellular K$^+$ also destabilizes the C-type inactivated state such that recovery from inactivation is accelerated with higher K$^+$ concentrations (14). These phenomena arise from a protective effect of extracellular permeant ions such as K$^+$, which can bind to external K$^+$ binding sites in the outer pore and prevent the structural rearrangements associated with C-type inactivation (15–18).

Previous studies have led to differing opinions regarding the possible voltage-dependence of C-type inactivation, and this may partially reflect heterogeneity of C-type inactivation mechanisms among different Kv channels (12). The current thinking for widely-studied channels such as *Shaker* and Kv2.1 is that upon membrane depolarization, S4 movement alters the conformation of the conduction pathway-lining S6 domain to open the channel. This conformational change is also suggested to disrupt interaction of S6 with the edge of the pore near the selectivity filter, destabilizing the open state of the inactivation gate, leading to C-type inactivation. It is

suggested that the S6 shift which constitutes opening, caused by S4 movement in response to voltage, indirectly bestows voltage-dependence upon C-type inactivation (19–22). However, because S4 movement is proposed to move S6 and also to alter the relative positions of S6 and the pore, it is difficult to discern which conformational shifts are required for C-type inactivation. Thus, it is difficult to distinguish whether C-type inactivation is a consequence of S6 movement, or alternatively a separate process initiated by S4 movement parallel to activation. This distinction is an important one; if the voltage-dependence of S6 movement is the only factor governing the voltage-dependence of C-type inactivation, the latter process lacks its own voltage-dependence and is dependent upon the voltage-dependence of activation for this property. Here, to examine these two alternatives, we exploited a constitutively-open Kv channel mutant to address the following questions: what type of inactivation can occur in a channel preopened by a voltage-independent process (i.e., the activation gate shifted to the open conformation without S4 movement); is the inactivation voltage-dependent or independent; and how does voltage-dependent movement of S4 impact any inactivation that occurs in this constitutively open channel?

Some form of inactivation is observed with the large majority of Kv channels; indeed, a lack of inactivation is rare. One example is the I_{Ks} complex, which is important for ventricular repolarization in human heart, and K^+ ion secretion into the endolymph of the inner ear (23–28). I_{Ks} is composed of the KCNQ1 α-subunit and the MinK (KCNE1) ancillary subunit (29,30). KCNQ1 is a six-transmembrane-domain Kv α-subunit from the S4 superfamily (26). MinK is the founding member of the KCNE gene family, which encodes single transmembrane domain ancillary subunits that associate with a range of Kv channels with diverse effects on channel function (31). Wild-type homomeric KCNQ1 channels exhibit voltage-gated activation and undergo weakly voltage-dependent inactivation which is not classic C-type inactivation because it is not sensitive to external K^+ concentration; coassembly with MinK removes this atypical inactivation (32–34).

The S6 domain of Kv channels lines the ion conduction pore and contains the activation gate, which moves after depolarization-initiated structural rearrangements of S4 to facilitate K^+ conduction (35). Most Kv channels contain a central S6 glycine which is thought to act as a gating hinge important for conformational changes in S6 during activation (36,37). KCNQ1 bears an alanine at this position (A336), probably reducing flexibility at this point compared to other Kv channels (38). Both *Shaker* and KCNQ1 contain another motif (PVP and PAG, respectively) nearer the intracellular end of S6 (residues 343–345 in KCNQ1) which also may endow flexibility and is proposed to be more important than the A/G hinge for S6 movement associated with activation of KCNQ1 (38) and perhaps *Shaker* (39,40). Between these two motifs lies the SFF 338–340 motif we previously found to be

crucial for mediating the effects of MinK and MiRPs on KCNQ1 activation (41). In particular, we and others found that F340 is required for MinK modulation of KCNQ1 activation via MinK T58, and that an F340W mutation uncouples MinK-KCNQ1 (I_{Ks}) channel activation from voltage, forming a constitutively open channel (41–43). Here we demonstrate that, paradoxically, F340W-I_{Ks} channels exhibit voltage-dependent inactivation bearing hallmarks of classic C-type inactivation. F340W-I_{Ks} channels thus represent a unique system in that they exhibit voltage-dependent C-type inactivation despite their constitutive activation. The properties of this voltage-dependent C-type inactivation, and its lack of dependence on voltage-dependent activation, are quantified and discussed here in the context of current models of inactivation in other Kv channels such as *Shaker*.

EXPERIMENTAL PROCEDURES

Molecular biology

Human KCNQ1 mutants were constructed using the QuikChange Multi Site-Directed Mutagenesis Kit (Stratagene, La Jolla, CA), and sequenced in their entirety to confirm correct sequence, then subcloned into a pBluescript-based oocyte expression vector. MinK cDNA was subcloned into the pRAT expression vector. cRNA transcripts were produced from *Not*I-linearized cDNA templates using the T3 (KCNQ1) and T7 (MinK) mMessage mMachine kits (Ambion, Austin, TX). cRNA was quantified by spectrophotometry and its size integrity verified by gel electrophoresis. Defolliculated stage V and VI oocytes from *Xenopus laevis* (Nasco, Fort Atkinson, WI) were injected with 10 ng of KCNQ1 with or without 2 ng of MinK cRNA.

Electrophysiology

Whole oocyte two-electrode voltage-clamp (TEVC) experiments were performed at room temperature using an OC-725C amplifier (Warner Instruments, Hamden, CT) and pClamp 9 software (Molecular Devices, Sunnyvale, CA), 3–4 days after cRNA injection. Oocytes were bathed in a small-volume oocyte bath (Warner) and viewed with a dissection microscope. Standard bath solution was (in mM): 96 NaCl, 4 KCl, 1 $MgCl_2$, 0.3 $CaCl_2$, 10 HEPES (pH 7.4) (4 K^+/96 Na^+ solution). TEVC pipettes were 1–2 $M\Omega$ resistance when filled with 3 M KCl. For analysis of the effects of different extracellular cations on inactivation, extracellular monovalent cations were replaced with 100 mM KCl, RbCl, CsCl, NaCl, or tetraethyl-ammonium (TEA) chloride where indicated. Data analysis was performed with pClamp 9 and Origin 6.1 (OriginLab, Northampton, MA). Values are stated as mean $\pm$ SE. For voltage-dependence of inactivation, tail currents or fractional decay during prepulse versus voltage were plotted and fit with single Boltzmann functions according to

$$I = \{A_1 - A_2/1 + \exp[(V_{1/2} - V)/V_s]\} + A_2, \qquad (1)$$

where I is the normalized current, A_1 is the initial value at $-\infty$, A_2 is the final value at $+\infty$, $V_{1/2}$ is the half-maximal voltage of activation, and V_s the slope factor (Origin 6.1). Inactivation traces were fitted with either a single or double-exponential function according to

$$I = \exp(-t/\tau_1), \qquad (2)$$

or

$$I = A_1\exp(-t/\tau_1) + A_2\exp(-t/\tau_2), \qquad (3)$$

where A_n is the initial amplitude of each component, t is time, and τ_n is the associated inactivation time constant of each component (pClamp 9).

Inactivation recovery traces were fitted with a single-exponential function according to

$$I = I_{peak}(1 - \exp[-t/\tau_{rec}]),　　　(4)$$

where τ_{rec} is the associated inactivation recovery time constant (pClamp 9).

According to the Goldman-Hodgkin-Katz (GHK) voltage equation,

$$E_{rev} = RT/F \ln \left(P_K[K]_o + P_{Na}[Na]_o + P_{Cl}[Cl]_i\right)/$$
$$\left(P_K[K]_i + P_{Na}[Na]_i + P_{Cl}[Cl]_o\right),　　(5)$$

where E_{rev} is the absolute reversal potential and P is permeability. This permits calculation of the relative permeability of each ion if concentrations on either side of the membrane are known. A modified version of this equation was used here to determine relative permeability of two ions in a system in which only the extracellular ion concentration was known. Thus, relative permeability of Rb$^+$, Cs$^+$, and Na$^+$ compared to K$^+$ ions was calculated for F340W-I$_{Ks}$ and R231A,F340W-I$_{Ks}$ channels by plotting the I/V relationships for each channel with each extracellular ion (100 mM) and comparing them to that with 100 mM extracellular K$^+$ ion to yield a change in reversal potential (ΔE_{rev}) for each ion compared to that of K$^+$. Permeability ratios for each ion (X) compared to K$^+$ were then calculated as

$$\Delta E_{rev} = E_{rev,X} - E_{rev,K+} = RT/zF \ln P_X/P_{K+}.　　(6)$$

Values were compared between channel types and statistical significance assessed using ANOVA. It is important to note that accurate measurement of reversal potentials can be hampered by a number of artifacts, including extracellular ion accumulation and leak currents. We attempted to keep these artifacts to a minimum by maintaining a high bath solution flow rate and discarding recordings for which current levels at -80 mV or $+80$ mV drifted significantly between pulses.

The gating charge involved in the inactivation process, z_i, of F340W-I$_{Ks}$ channels was estimated using two independent methods. First, a linear regression analysis of the reciprocal of $\tau_{inactivation}$ (inactivation rate constant) versus V_{test} was used as

$$\ln[K(V_{test})] = \ln[K(0)] + z_i V_{test}(F/RT),　　(7)$$

where $K(V_{test})$ and $K(0)$ are the rate constants of inactivation at voltages V_{test} and 0 mV, respectively, and $F/RT = 0.04$ mV^{-1}. This approximation of the rate constant for inactivation holds for voltages at which recovery from inactivation is negligible. Second, z_i was estimated from the slope of the Boltzmann fit of the plot of inactivation-recovered current versus recovery voltage using the partial recovery inactivation protocol, thus,

$$z_i = \text{slope}/(RT/F),　　(8)$$

where $RT/F = 25$ mV.

Structural models

For Fig. 1, D and E, substitution of KCNQ1 phenylalanine 340 for tryptophan was applied to the equivalent position in the Kv1.2 ROSETTA open-state model for which coordinates were kindly provided by Yarov-Yarovoy et al. (44). Molecular model images were prepared using PyMOL (http://pymol.sourceforge.net/). Homology modeling of the KCNQ1 S4 and S4–S5 linker domains (see Fig. 12 C) was performed with the SWISS-MODEL program (45) using structural coordinates from x-ray crystallographic studies of similar domains in Kv1.2 as a template (46). Images were prepared using PROTEIN EXPLORER ALPHA.

RESULTS

F340W-I$_{Ks}$ channels are constitutively open and exhibit inactivation

The functional properties of wild-type and mutant KCNQ1 α-subunits, alone or coexpressed with MinK, were assessed using TEVC studies of the channels expressed in *Xenopus* oocytes, initially with a bath solution containing 4 mM KCl and 96 mM NaCl. Coassembly with MinK ancillary subunits has several functional effects on wild-type KCNQ1 α-subunits: a fourfold increase in unitary conductance, significant slowing of activation, a positive shift in the voltage dependence of activation, and loss of inactivation (29,30,47) (Fig. 1, A–C). Inactivation of homomeric KCNQ1 channels is modest but can be detected by a hook in currents recorded during the tail pulse due to recovery from inactivation before deactivation occurs; this hook is absent from tail currents generated by wild-type KCNQ1-MinK (I$_{Ks}$) channels (33,34).

Previously, we found that an F340W mutation in the S6 domain of KCNQ1 results in partially constitutive activation of homomeric KCNQ1 channels and essentially entirely constitutive activation in F340W-I$_{Ks}$ channels (41). KCNQ1-F340 is situated in the MiRP-interaction domain halfway along the S6 pore-lining helix close to other motifs thought important for conformational changes in S6 during activation (Fig. 1 D). Aligning the KCNQ1 and *Shaker* sequences, F340 is predicted to sit below the selectivity filter with each aromatic ring facing toward the adjoining α-subunit in a clockwise fashion (viewed from the extracellular side) based on a ROSETTA open-state model derived from the crystal structure of Kv1.2 (44,48), (Fig. 1, D and E). Strikingly, channels bearing the F340W mutation exhibited current decay at depolarized voltages, suggestive of voltage-dependent inactivation, despite constitutive (voltage-independent) activation (Fig. 1 F). Rather than being removed by MinK as in wild-type I$_{Ks}$ complexes, inactivation was actually more comprehensive in F340W-I$_{Ks}$ channels than in homomeric F340W-KCNQ1 channels, resulting in particularly robust inward rectification in the former, as shown by comparing peak versus steady-state I/V relationships (Fig. 1, G and H). For the remainder of this study of the voltage dependence of inactivation, we therefore generally employed F340W-I$_{Ks}$ channels.

F340W-I$_{Ks}$ inactivation is voltage-dependent

The voltage dependence of F340W-I$_{Ks}$ inactivation was immediately apparent upon examination of standard current-voltage families: F340W-I$_{Ks}$ channels exhibited inward rectification, reducing current at more depolarized voltages (Fig. 1, G and H; Fig. 2 A) reminiscent of hERG channels in which inward rectification arises from rapid inactivation upon depolarization (49). Current decay was absent at hyperpolarized voltages but readily apparent at depolarized voltages, suggesting a form of inactivation that was voltage-dependent, in contrast to activation which was voltage-independent (Fig. 2 A). F340W-I$_{Ks}$ channels behave quite distinctly from wild-type I$_{Ks}$ channels. MinK eliminates inactivation of wild-type KCNQ1 channels, in contrast to our observations for F340W-I$_{Ks}$ channels (33,34). Onset of inactivation of homomeric wild-type KCNQ1 channels is delayed upon depolarization, suggesting the necessity for transition through more than one
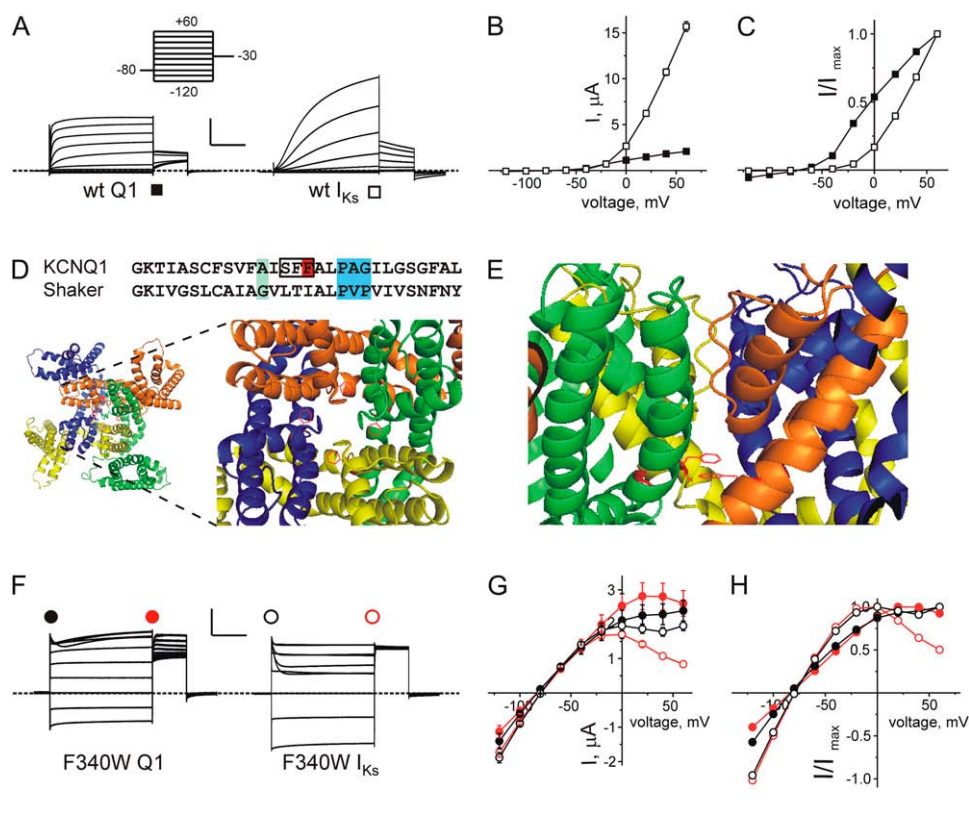
FIGURE 1 F340W-I_{Ks} channels are constitutively open but exhibit voltage-dependent inactivation. (*A*) Exemplar current traces recorded in oocytes expressing wild-type KCNQ1 alone (wt Q1) or with MinK (wt I_{Ks}) channels as indicated. Currents were recorded by TEVC using the standard voltage family protocol (*inset*). (*Scale bars*) Vertical, 1 μA (wt Q1), 3 μA (wt Q1 + MinK); and horizontal, 1 s. (*Dashed line*) Zero current level. (*B*) Raw I/V relationships, measured at the end of the test pulse, for oocytes as in panel *A*, $n = 7$–10. Symbols as in panel *A*. Error bars indicate SEM. Data were fitted with a Boltzmann function. (*C*) Normalized I/V relationships for oocytes as in panel *A*, $n = 7$–10. Symbols as in panel *A*. Error bars indicate SEM. Data were fitted with a Boltzmann function. (*D*) (*Upper*) Sequence alignment of the KCNQ1 and *Shaker* S6 domains. (*Green*) Postulated glycine hinge in *Shaker* (37); mutation of the KCNQ1 alanine at this position to glycine may increase flexibility (38). (*Red*) F340W. (*Boxed region*) S338-F340 MiRP interaction domain (41). (*Blue*) PAG/PVP postulated flexible activation gate region (38,40). (*Lower*) View from the extracellular side of the Kv$_{1.2}$ structure open-state model (44) with the position homologous to KCNQ1-F340 shown as a phenylalanine and highlighted red. (*Left*) Entire channel; (*right*) closeup of pore region. (*E*) Lateral projection of the Kv$_{1.2}$ structure open-state model with the residue homologous to KCNQ1-F340 shown as a phenylalanine and highlighted red, demonstrating its predicted position below the selectivity filter. (*F*) Exemplar current traces recorded in oocytes expressing F340W-KCNQ1 alone (F340W Q1) or with MinK (F340W I_{Ks}) channels as indicated. Currents recorded as in panel *A*. (*Scale bars*) Vertical, 1 μA; horizontal, 1 s. Zero current level indicated by dashed line. (*G*) Raw instantaneous (*solid black* or *open* with *black border*) and steady-state (*solid red* or *open* with *red border*) I/V relationships for oocytes as in panel *F*, $n = 8$–10. (*Solid symbols*) F340W KCNQ1; (*open symbols*) F340W I_{Ks}. Error bars indicate SEM. (*H*) Normalized instantaneous (*solid black* or *open* with *black border*) and steady-state (*solid red* or *open* with *red border*) I/V relationships for oocytes as in panel *F*, $n = 8$–10. (*Solid symbols*) F340W KCNQ1; (*open symbols*) F340W I_{Ks}. Error bars indicate SEM.

type of open state before inactivation can occur (33). In contrast, inactivation of F340W-I_{Ks} channels proceeded without perceptible delay upon depolarization (Fig. 2 *A*).

Extent of inactivation of F340W-I_{Ks} channels was quantified by two methods, revealing voltage dependence such that the extent of inactivation increased with depolarization. First, visible fractional decay was plotted versus voltage; fitting of fractional decay versus voltage with a Boltzmann function gave a $V_{1/2 \text{ inactivation}}$ of 37.1 $\pm$ 1.9 mV, slope of 22.3 $\pm$ 1.4 mV, and amplitude of 0.87 $\pm$ 0.03 (Fig. 2 *C*, *solid squares*). Second, a partial recovery protocol was employed such that inactivation was permitted to reach steady-state at +80 mV, followed by a brief (20 ms) recovery phase at various voltages then a +80 mV tail pulse for quantification of the equilibrium between inactivated and noninactivated channels as a function of recovery step voltage (Fig. 2 *B*). Fitting the extent of inactivation versus voltage relationship with a Boltzmann function gave a $V_{1/2 \text{ inactivation}}$ of $-17.0 \pm$ 4.1 mV, slope of 26.3 $\pm$ 3.4 mV, and amplitude of 0.75 $\pm$ 0.04 (Fig. 2 *C*). The slope of this Boltzmann fit was used to estimate the gating charge of inactivation, z_i, using Eq. 8,

giving a value of 1.05. The $V_{1/2}$ of activation for wild-type I_{Ks} was previously calculated as 20 $\pm$ 3 mV, closest to our more depolarized value for the $V_{1/2}$ of inactivation (29,30,47).

The substantial shift in calculated voltage dependence with these two fits may arise from the fact that the partial recovery double-pulse protocol does not permit complete recovery from inactivation before the tail current is measured, and/or that quantifying inactivation using the visible current decay omits inactivation so rapid it cannot be visualized using two-electrode voltage-clamp. Alternatively, it could reflect adoption of a more stable C-type inactivated state with the double-pulse protocol (Fig. 2 *B*) by virtue of the long pre-pulse to +80 mV before the recovery step (Fig. 2 *B*), whereas the prepulse of -80 mV in the decay protocol (Fig. 2 *A*) delays adoption of this more stable state. The adoption of a more stable C-type inactivated state involving gating charge immobilization was previously found for the Kv1.5 channel (50). We consider it likely, however, that there is an underestimation using the visible decay measurement and therefore for the majority of this study we compare inactivation voltage-dependence and extent using the double-pulse protocol.
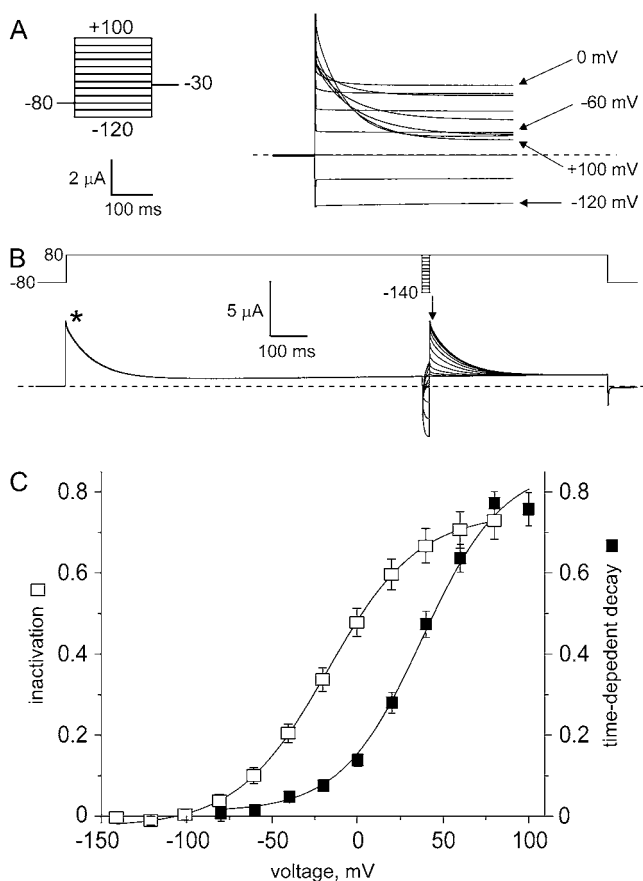
FIGURE 2 F340W-I_{Ks} channels exhibit voltage-dependent inactivation. (*A*) First 500 ms of exemplar traces recorded in oocytes expressing F340W-I_{Ks} with 4 K⁺/96 Na⁺ bath solution using a similar protocol to that in Fig. 1 (*inset*); note instantaneous onset of inactivation at membrane potentials from −20 to +100 mV. (*Dashed line*) Zero current level. (*B*) Exemplar traces recorded in oocytes expressing F340W-I_{Ks} with 4 K⁺/96 Na⁺ bath solution using a partial recovery protocol incorporating a 1 s pulse to +80 mV followed by a 20-ms inactivation recovery step to voltages between −140 and +80 mV, then a 500 ms +80 mV tail pulse (protocol above). (*Dashed line*) Zero current level. (*C*) (*Solid squares*) Visible fractional current decay during test pulses as in panel *A*, $n = 8–10$. (*Open squares*) Inactivation quantified by plotting (1 − normalized peak tail current). Peak tail current (*arrow, B*) was normalized to peak prepulse current (*asterisk, B*), $n = 14$. Data were fitted with a Boltzmann function for both data sets (*solid lines*). Error bars indicate SEM.

Voltage dependence of F340W-I_{Ks} inactivation kinetics

In voltage-activated potassium channels, inactivation rate has not previously been found to be intrinsically voltage-dependent, purportedly because this correlation was masked by the voltage dependence of activation (13). Here, we fitted the kinetics of F340W-I_{Ks} inactivation between −40 and 0 mV, a range of voltages over which decay was visible but inward rectification (caused by loss of the peak due apparently to inactivation) was minimal, to limit as much as possible underestimation of inactivation rate (Fig. 3 *A*). Inactivation rate, fitted with a double-exponential function, was voltage-dependent such that the time constant of the slow component of inactivation, τ_1, became faster with depolarization. The voltage dependence of τ_1 was fit with a Boltzmann function, yielding a $V_{1/2}$ of −17.5 ± 4.8 mV, V_s of 6.8 ± 5.6 mV, $A_1 = 222.9 \pm 44.0$ ms, and $A_2 = 39.4 \pm 29.5$ ms (where A_1 and A_2 indicate the fractional amplitudes of current decaying by τ_1 and τ_2, respectively). In contrast, the time component of the fast component of inactivation (τ_2) appeared voltage-independent and had a constant value of ~20 ms over the range tested (Fig. 3 *B*). Thus in the absence of voltage-dependent opening, the voltage-dependence of inactivation kinetics was demonstrable. The relative contribution of A_1 exhibited apparent *v*-shaped voltage dependence with a minimum of ~0.3 at −20 mV (Fig. 3 *C*). We interpret this as introduction or unmasking of a very fast component to inactivation above −20 mV that probably underlies the inward rectification observed for peak currents (Fig. 2 *A*); therefore, A_1 in reality may continue to drop above −20 mV. The voltage dependence of the reciprocal of the slow component of inactivation, τ_1 (an approximation of the rate constant for the slow component of inactivation) was subjected to linear regression analysis to estimate z_i using Eq. 7. It should be noted that this method of determining the rate constant for inactivation is accurate only for voltages at which there is negligible recovery from inactivation, and also that visible decay may not represent all the voltage-dependent inactivation occurring. The calculated z_i value should therefore be treated with caution; however, this method yielded a z_i of 0.84, similar to the value of 1.05 yielded using Eq. 8.

F340W-I_{Ks} inactivation recovery kinetics is voltage-dependent

The kinetics of recovery from inactivation can prove difficult to evaluate because of concomitant deactivation resulting in superimposed current decay at hyperpolarized voltages (49,51). Here, the F340W-I_{Ks} channel facilitated assessment of the kinetics of recovery from inactivation in the absence of deactivation. Inactivation recovery traces were recorded at various voltages after a +80 mV prepulse (Fig. 3 *D*). Fitting of inactivation recovery traces with a single exponential function demonstrated that the rate of recovery from inactivation of F340W-I_{Ks} channels was strongly voltage-dependent: recovery at −140 mV was 10-fold faster than at 0 mV (Fig. 3 *E*).

Extracellular permeant cations antagonize F340W-I_{Ks} inactivation

Inactivation of homomeric wild-type KCNQ1 channels—not considered to be typical C-type inactivation—is unaffected by increasing external K⁺ concentration (33,34), whereas the classic C-type inactivation of *Shaker* and similar forms of inactivation in Kv channels such as Kv1.5 are sensitive to external K⁺ ion concentration, with high external K⁺ con-
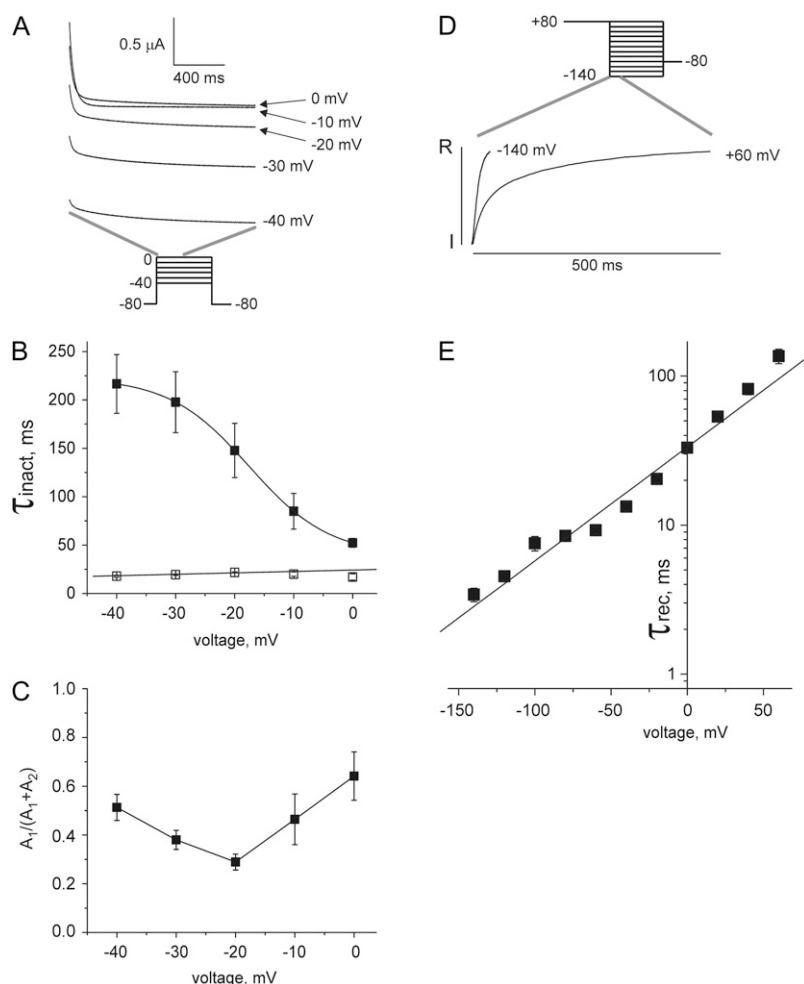
FIGURE 3 Voltage dependence of F340W-I_{Ks} inactivation and inactivation recovery kinetics. (*A*) First 1.5 s of exemplar traces recorded in oocytes expressing F340W-I_{Ks} with 4 K^+/96 Na^+ bath solution using the protocol inset. (*B*) Mean inactivation rate plotted as τ_1 (*solid squares*) and τ_2 (*open squares*) of a double-exponential fit of traces as in panel *A*, $n = 11$. Error bars indicate SEM. (*C*) Mean relative amplitude of the slow component of inactivation as a fraction of total amplitude, $A_1/(A_1 + A_2)$, plotted versus voltage, for traces as in panel *A* after a double-exponential fit, $n = 11$. Error bars indicate SEM. (*D*) First section of normalized inactivation recovery tail currents (-140 and $+60$ mV) of exemplar traces recorded in oocytes expressing F340W-I_{Ks} with 4 K^+/96 Na^+ bath solution using the protocol inset. (*I*) Inactivated; (*R*) recovered. (*E*) Inactivation recovery rate plotted as the τ of a single-exponential fit of traces as in panel *D*, $n = 6$. Error bars indicate SEM.

centration antagonizing inactivation. Furthermore, antagonism of C-type inactivation positively correlates with the relative permeability of the predominant monovalent cation on the extracellular side. Both these phenomena are thought to be due to prevention of pore collapse by binding of permeant ions to external pore ion binding sites (8,13,15,52–55). Here, we tested the effects of replacing the 4 K^+/96 Na^+ bath solution with one containing a single monovalent cation species at 100 mM, which was either K^+, Rb^+, Cs^+, Na^+, or TEA^+. The TEA^+ sensitivity of I_{Ks} channels is extremely low, with an estimated $IC_{50} > 100$ mM (56); thus here we were able to utilize TEA^+ as a relatively impermeant ion, rather than as a pore-blocker with a high-affinity external binding site as is the case with many other Kv channels (13,55,57–59).

Recording of current families from oocytes expressing F340W-I_{Ks} and replacing the bath solution in turn showed that 100 mM K^+, Rb^+, Cs^+, or Na^+ increased the mean instantaneous outward currents relative to those with the 4 K^+/96 Na^+ bath solution whereas 100 mM TEA^+ did not (Fig. 4, *A* and *B*). The increase in instantaneous current with 100 mM K^+ compared to that with 4 mM K^+ was particularly significant since the increased external K^+ represents a marked reduction in chemical gradient and would be predicted to decrease outward current. Steady-state inactivated outward current, measured at the end of the 3-s test pulse, was significantly increased by 100 mM K^+, Rb^+, and Cs^+, but not Na^+ or TEA^+ (Fig. 4 *C*). Both the increase in late current amplitude with 100 mM K^+ and lack of increase in late current amplitude with 100 mM Na^+ are highly significant because, again, they are contrary to what would be expected from the effects of driving force. The increase in outward current at depolarized voltages when permeant ions dominated the extracellular milieu: K^+, Rb^+ and even Cs^+ (discussed later, see Fig. 11) was of greater magnitude the more depolarized the membrane potential, 5–10-fold greater than the current observed with the 4 K^+/96 Na^+ solution at $+60$ mV (Fig. 4 *D*). These effects were characteristic of a channel that undergoes classic C-type inactivation because, as explained, this process is antagonized by an increase in the concentration of permeant extracellular cations, which disfavors pore constriction. With Na^+ as the sole extracellular monovalent cation, steady-state current was similar to that for 4 mM K^+ despite the increased driving force and in contrast to the threefold increase in instantaneous current compared to with 4 mM K^+ (Fig. 4, *B–D*); this again was highly consistent
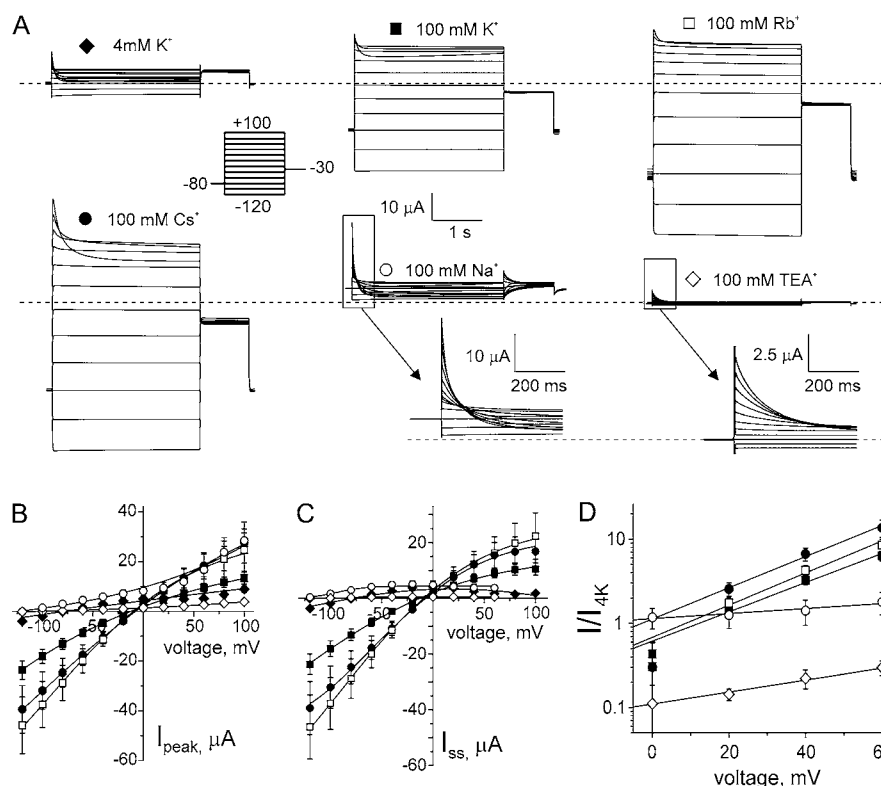
FIGURE 4 Effect of external permeant ions on F340W-I_{Ks} currents. (*A*) Exemplar current traces recorded in an oocyte expressing F340W-I_{Ks} channels using the protocol inset. Bath solution was varied such that the monovalent cations comprised 4 mM K$^+$/96 mM Na$^+$, or 100 mM K$^+$, Rb$^+$, Cs$^+$, Na$^+$, or TEA$^+$ as indicated. For Na$^+$ and TEA$^+$ currents, insets (*arrows*) show magnification of boxed region. Central scale bars apply to all traces except for insets, which have their corresponding scale bars. (*Dashed lines*) Zero current level. (*B*) Raw *I/V* relationships for peak currents from oocytes as in panel *A*, $n = 8$–12. Symbols as in panel *A*. Error bars indicate SEM. (*C*) Raw *I/V* relationships for late currents (end of 3 s test pulse) from oocytes as in panel *A*, $n = $ 8–12. Symbols as in panel *A*. Error bars indicate SEM. (*D*) Late currents from oocytes as in panel *A* normalized to late current using 4 K$^+$/96 Na$^+$ bath solution, between 0 and +60 mV; $n = 8$–12. Error bars indicate SEM.

with a lack of protection of the pore from constriction associated with time- and voltage-dependent inactivation. TEA$^+$ resulted in threefold reduced instantaneous and fivefold reduced steady-state current density (Fig. 4, *B–D*), most likely due to a combination of weak block and a lack of protection from pore constriction during C-type inactivation. TEA$^+$ protects some channels from C-type inactivation by a foot-in-the-door mechanism, but the extremely low TEA affinity of I_{Ks} (56) likely prevents this protective effect.

The effects on F340W-I_{Ks} inactivation of varying the extracellular ionic milieu were apparent from normalized traces at +80 mV, showing only 10–25% decay with 100 mM K$^+$, Rb$^+$, or Cs$^+$, compared to 80–90% decay with 100 mM Na$^+$ or TEA$^+$, or 4 K$^+$/96 Na$^+$ (Fig. 5 *A*). Further, normalized mean steady-state I/V curves from groups of oocytes bathed in either of the latter three solutions showed much stronger inward rectification than with 100 mM K$^+$, Rb$^+$, or Cs$^+$, due to the voltage- and extracellular cation-dependence of inactivation (Fig. 5 *B*). A plot of fractional decay versus voltage with the various bath solutions demonstrated that inactivation was less extensive at a given voltage the higher the permeability of the predominant extracellular cation (Fig. 5 *C*). Put another way, compared to currents with 4 K$^+$/96 Na$^+$ bath solution, 100 mM Na$^+$, or TEA$^+$ left-shifted the voltage-dependence of fractional current decay ~50 mV, whereas 100 mM K$^+$, Rb$^+$, or Cs$^+$ right-shifted fractional current decay in excess of 50 mV (Fig. 5 *C*).

Quantification of inactivation using the 20-ms partial recovery protocol (Fig. 5, *D* and *E*) demonstrated dramatic

negative shifts in the voltage-dependence of inactivation compared to 4 K$^+$/96 Na$^+$ recordings with 100 mM Na$^+$ (−60 mV shift) or TEA$^+$ (−90 mV shift) extracellular solution. In 100 mM extracellular K$^+$, Rb$^+$, or Cs$^+$, inactivation was positive-shifted such that <10% inactivation was observed at +60 mV, and voltage-dependence could not be quantitatively fitted (Fig. 5 *E*). These data, even more polarized than for fractional decay data in Fig. 5 *C*, suggested profound shifts in the kinetics of inactivation recovery during the variable-voltage 20-ms recovery step (Fig. 5 *D*), quantification of which is described in Fig. 6.

Voltage dependence of F340W-I_{Ks} inactivation kinetics with impermeant extracellular cations

F340W-I_{Ks} inactivation kinetics appeared voltage-dependent, with faster inactivation at more depolarized voltages, even in the absence of extracellular K$^+$ ions (Fig. 4). This was quantified for currents recorded with either Na$^+$ or TEA$^+$ (100 mM) as the sole extracellular monovalent cation. Traces recorded with other extracellular ions exhibited only relatively small amounts of very slow inactivation, precluding accurate fitting of kinetics. Inactivation rate, fitted with a double-exponential function, was voltage-dependent such that both the slow (τ_1) and fast (τ_2) components of inactivation became approximately threefold faster between −40 and +100 mV with either Na$^+$ or TEA$^+$ (Fig. 6 *A*). The contribution of limiting time constant A_1 increased from 0.5 to 0.7 for Na$^+$ between −40 and +100 mV, and varied
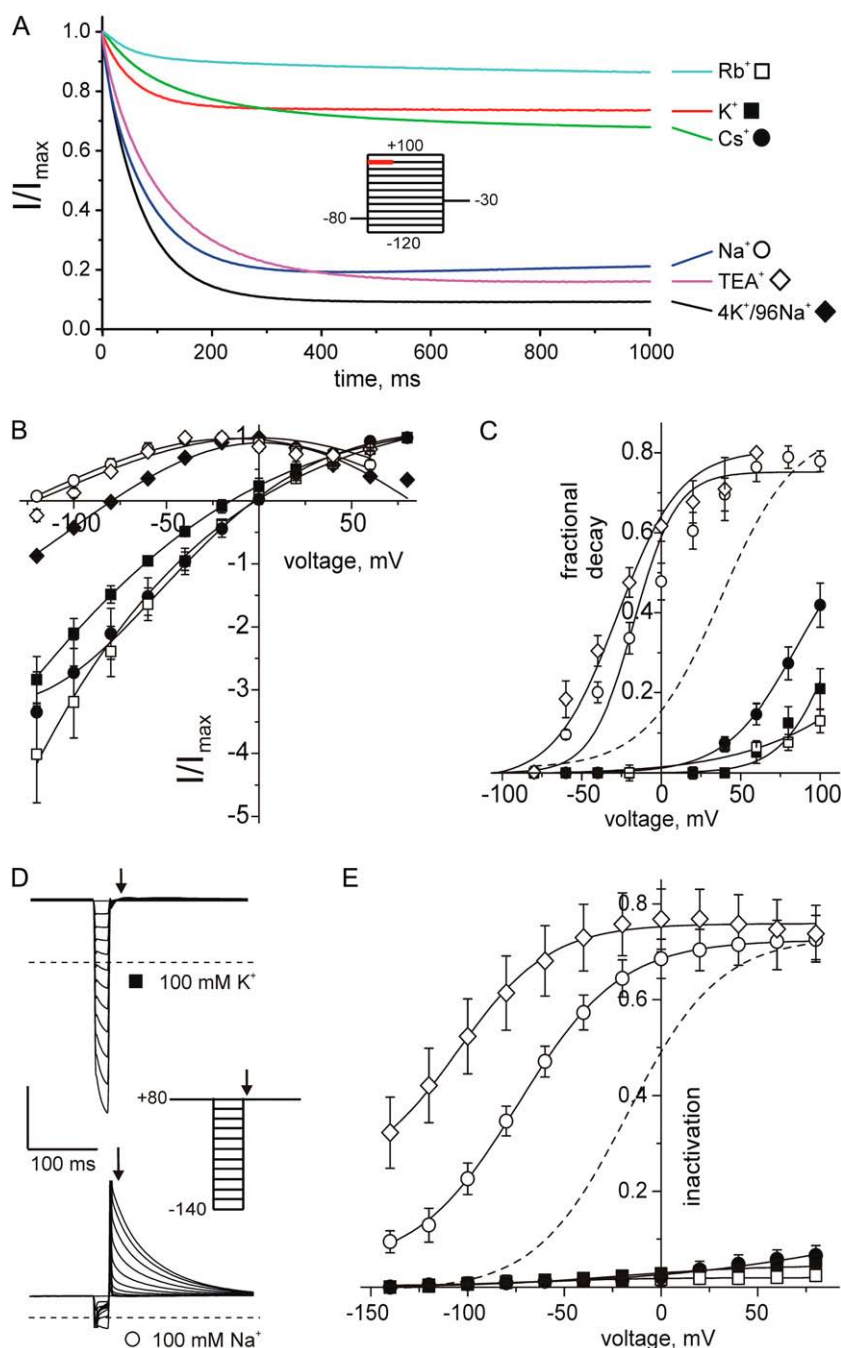
FIGURE 5 Effect of external permeant ions on F340W-I_{Ks} inactivation. (*A*) Normalized exemplar current traces recorded at +80 mV in oocytes expressing F340W-I_{Ks} channels using the protocol inset (*traces* correspond to region indicated by *red bar* in protocol) showing different degrees of current decay depending on external ion species. Bath solution was varied such that the monovalent cations comprised 4 mM K$^+$/96 mM Na$^+$, or 100 mM K$^+$, Rb$^+$, Cs$^+$, Na$^+$, or TEA$^+$ as indicated. (*B*) Normalized *I/V* relationships for late currents (end of 3-s test pulse) from oocytes as in panel *A*, $n = 8$–12. Symbols and protocol as in panel *A*. Error bars indicate SEM. (*C*) Inactivation quantified as visible fractional current decay during test pulses as in panel *A*, $n = 8$–12. Error bars indicate SEM. Data were fitted with a Boltzmann function, showing that inactivation varied with external ion species. Fit values were obtainable for Cs$^+$, Na$^+$, and TEA$^+$ experiments, as follows. Cs$^+$: A_1, 0.0 ± 0.001; A_2, 0.62 ± 0.32; $V_{0.5}$, 85.0 ± 24.1 mV; and V_s, 22.0 ± 6.9 mV. Na$^+$: A_1, 0.0 ± 0.0; A_2, 0.75 ± 0.02; $V_{0.5}$, -17.2 ± 2.2 mV; and V_s 13.3 ± 0.7 mV. TEA$^+$: A_1, 0.0 ± 0.02; A_2, 0.81 ± 0.01; $V_{0.5}$, -27.4 ± 2.5 mV, and V_s, 19.8 ± 2.3 mV. (*Dashed line*) Fit for 4 K$^+$/96 Na$^+$ data for comparison. (*D*) Central 400 ms of exemplar traces recorded in oocytes expressing F340W-I_{Ks} with 100 mM external bath cations as indicated, using a partial recovery protocol incorporating a 1 s pulse to +80 mV followed by a 20-ms inactivation recovery step to voltages between -140 and +80 mV, then a 500 ms +80 mV tail pulse (*inset*). (*Dashed lines*) Zero current level. Vertical scale bar indicates 19 μA (K$^+$), 16 μA (Na$^+$). (*E*) Inactivation quantified by plotting $1 -$ normalized tail current at arrow (*D*), $n = 4$–12. Symbols as in panel *A*. Data were fitted with a Boltzmann function. Error bars indicate SEM. (*Dashed line*) Inactivation fit from 4 K$^+$/96 Na$^+$ recordings for comparison. Fit values were obtainable for Na$^+$ and TEA$^+$ experiments, as follows. Na$^+$: A_1, 0.04 ± 0.05; A_2, 0.72 ± 0.03; $V_{0.5}$, -73.9 ± 5.6 mV; and V_s, 26.4 ± 5.5 mV; and TEA$^+$: A_1, 0.23 ± 0.29; A_2, 0.76 ± 0.03; $V_{0.5}$, -105.0 ± 32.4 mV; and V_s, 23.7 ± 17.4 mV.

between 0.7 and 0.8 for TEA$^+$ (Fig. 6 *B*; see Fig. 6 legend for fit values). Thus in the absence of extracellular K$^+$ or other relatively permeant extracellular cations, F340W-I_{Ks} inactivation was still voltage-dependent.

Extracellular permeant cations accelerate recovery from inactivation of F340W-I_{Ks}

The kinetics of inactivation recovery were also affected by the extracellular monovalent cation species, such that more permeant ions (100 mM K$^+$, Rb$^+$, and to a lesser extent Cs$^+$)

accelerated recovery and less permeant ions (100 mM Na$^+$) retarded recovery compared to the 4 K$^+$/96 Na$^+$ bath solution. This manifested as a negative shift in the voltage dependence of recovery kinetics with 100 mM Na$^+$ and a positive shift for 100 mM K$^+$, Rb$^+$, or Cs$^+$, compared to with the 4 K$^+$/96 Na$^+$ solution (Fig. 6, *C* and *D*). Recovery rates with 100 mM K$^+$ or Rb$^+$ were 10-fold higher than with the 4 K$^+$/96 Na$^+$ bath solution at +60 mV. Currents were too small for reliable assessment of recovery with TEA$^+$ as the extracellular monovalent cation. Overall, the positive correlation between inactivation recovery rate and relative permeability of external
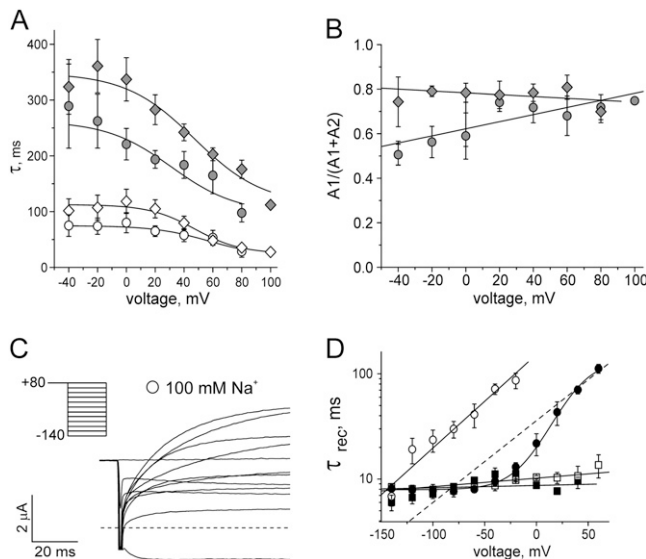
FIGURE 6 Voltage and external cation dependence of F340W-I$_{Ks}$ inactivation and inactivation recovery kinetics. (A) Inactivation rate plotted as the τ-values from a double-exponential fit of inactivation versus voltage from traces as in Fig. 4 A, n = 6–7. (Circles) 100 mM Na$^+$; (diamonds) 100 mM TEA$^+$. (Shaded symbols) $\tau 1$; (open symbols) $\tau 2$. Error bars indicate SEM. Voltage dependence of each τ-value was fit with a Boltzmann function. Na$^+$ τ_1: $V_{1/2} = 31.3 \pm 20.2$ mV; $V_s = 22.6 \pm 11.3$ mV; $A_1 = 267.9 \pm 57.1$ ms; and $A_2 = 97.7$ ms, fixed automatically by fitting software. Na$^+$ τ_2: $V_{1/2} = 49.7 \pm 16.1$ mV; $V_s = 16.1 \pm 12.6$ mV; $A_1 = 74.5 \pm 11.2$ ms; and $A_2 = 28.8$ ms, fixed automatically by fitting software. TEA$^+$ τ_1: $V_{1/2} = 47.3 \pm 9.9$ mV; $V_s = 23.9 \pm 6.4$ mV; $A_1 = 348.7 \pm 38.4$ ms; and $A_2 = 112.1$ ms, fixed automatically by fitting software. TEA$^+$ τ_2: $V_{1/2} = 47.6 \pm 8.3$ mV; $V_s = 15.9 \pm 5.4$ mV; $A_1 = 112.6 \pm 13.9$ ms; and $A_2 = 24.8 \pm 4.3$ ms. (B) Mean relative amplitude of the slow component of inactivation as a fraction of total amplitude, $A_1/(A_1 + A_2)$, plotted versus voltage, after double-exponential fit of inactivation from traces as in Fig. 4 A, n = 6–7. (Circles) 100 mM Na$^+$; (diamonds) 100 mM TEA$^+$. Error bars indicate SEM. (C) First section of normalized inactivation recovery tail currents of exemplar traces recorded in oocytes expressing F340W-I$_{Ks}$ with 100 mM external Na$^+$ ion, using the protocol inset. (Dashed line) Zero current level. (D) Inactivation recovery rate plotted as the τ of a single-exponential fit of the recovery phase (τ_{rec}) from traces as in panel C, with 100 mM external Na$^+$ (open circles), K$^+$ (solid squares), Cs$^+$ (solid circles), or Rb$^+$ (open squares); n = 3–6. Error bars indicate SEM. (Dashed line) Fit from 4 K$^+$/96 Na$^+$ recordings for comparison. Recovery currents above 0 mV were too small to quantify for 100 mM K$^+$ and 100 mM Rb$^+$ recordings.

monovalent cations was similar to that observed for Shaker and typical of classic C-type inactivation (14).

S4 charge provides the voltage-dependence of F340W-I$_{Ks}$ inactivation

The voltage-dependent C-type inactivation with physiological concentrations of intracellular and extracellular ions and in the absence of voltage-dependent activation observed for F340W-I$_{Ks}$ channels was suggestive of coupling between the C-type inactivation gate and an intrinsic voltage sensor. To test the contribution of S4, the voltage sensor for activation in wild-type I$_{Ks}$ and other Kv channels, we performed alanine-

scanning mutagenesis of charged residues in the S4 and adjoining linkers (S3-S4 and S4-S5) of F340W-I$_{Ks}$ (Fig. 7 A). Each of two individual S4 charge neutralizations altered the inactivation of F340W-I$_{Ks}$ channels. Thus, unlike the majority of S4 mutants and single mutant F340W-I$_{Ks}$ channels, R231A,F340W-I$_{Ks}$ channels showed a linear I/V curve with no current decay during the 3 s test pulse between −120 and +40 mV (Fig. 7, B–D, but see Figs. 9–11 for evidence of constitutive inactivation). R237A,F340W-I$_{Ks}$ channels exhibited no visible current decay but there was a clear voltage-dependence to activation, and a time-dependent component to activation was apparent at depolarized voltages, unlike single-mutant F340W-I$_{Ks}$ channels (Fig. 7, B–D). These data demonstrate that S4 is involved in the development of C-type inactivation in F340W-I$_{Ks}$ and that charged residues R231 and R237 are particularly important for this process.

We interpret these effects as highly suggestive that S4 acts as the voltage sensor for C-type inactivation in F340W-I$_{Ks}$, although strictly in the absence of a quantitative relationship between the number of S4 charges and the voltage-dependence of inactivation, another possible interpretation is that S4 is involved for example in coupling voltage sensing to inactivation rather than acting as the voltage sensor itself. However, the current findings for R231 and R237 mirror the importance of these residues in voltage-dependent activation of wild-type I$_{Ks}$ channels (60) suggesting a common structural element, S4, provides both the voltage dependence of inactivation in F340W-I$_{Ks}$ channels in the absence of voltage-dependent activation, and the voltage dependence of activation in wild-type I$_{Ks}$.

S4-S5 linker charge influences C-type inactivation of F340W-I$_{Ks}$

The S4-S5 linker is essential for coupling of S4 movement to the activation gate in Kv channels including Shaker and wild-type I$_{Ks}$ and also mediates functional interaction between MinK and KCNQ1 in wild-type I$_{Ks}$ complexes (61,62). Here, neutralization of a single S4-S5 linker charge, E261, significantly reduced the inward rectification of F340W-I$_{Ks}$ channels (Fig. 7, B and D). Quantification of current decay during the 3-s test pulse showed that the E261A,F340W mutant reduced decay approximately twofold at +40–+60 mV compared to single-mutant F340W-I$_{Ks}$ channels and other charge mutants that showed any decay (i.e., those other than R231A,F340W and R237A,F340W) (Fig. 7 E). An alternative measure of inactivation in which percentage of channels available at the start of the tail pulse was compared to total channels available (peak current during test pulse) showed qualitatively similar effects (Fig. 7 F). This reduced inactivation for E261A,F340W-I$_{Ks}$ during the test pulse was attributable to a fivefold reduction in inactivation rate at +60 mV, estimated for comparison purposes from a single-exponential fit of single- and double-mutant F340W-I$_{Ks}$ channels (Fig. 7 G).
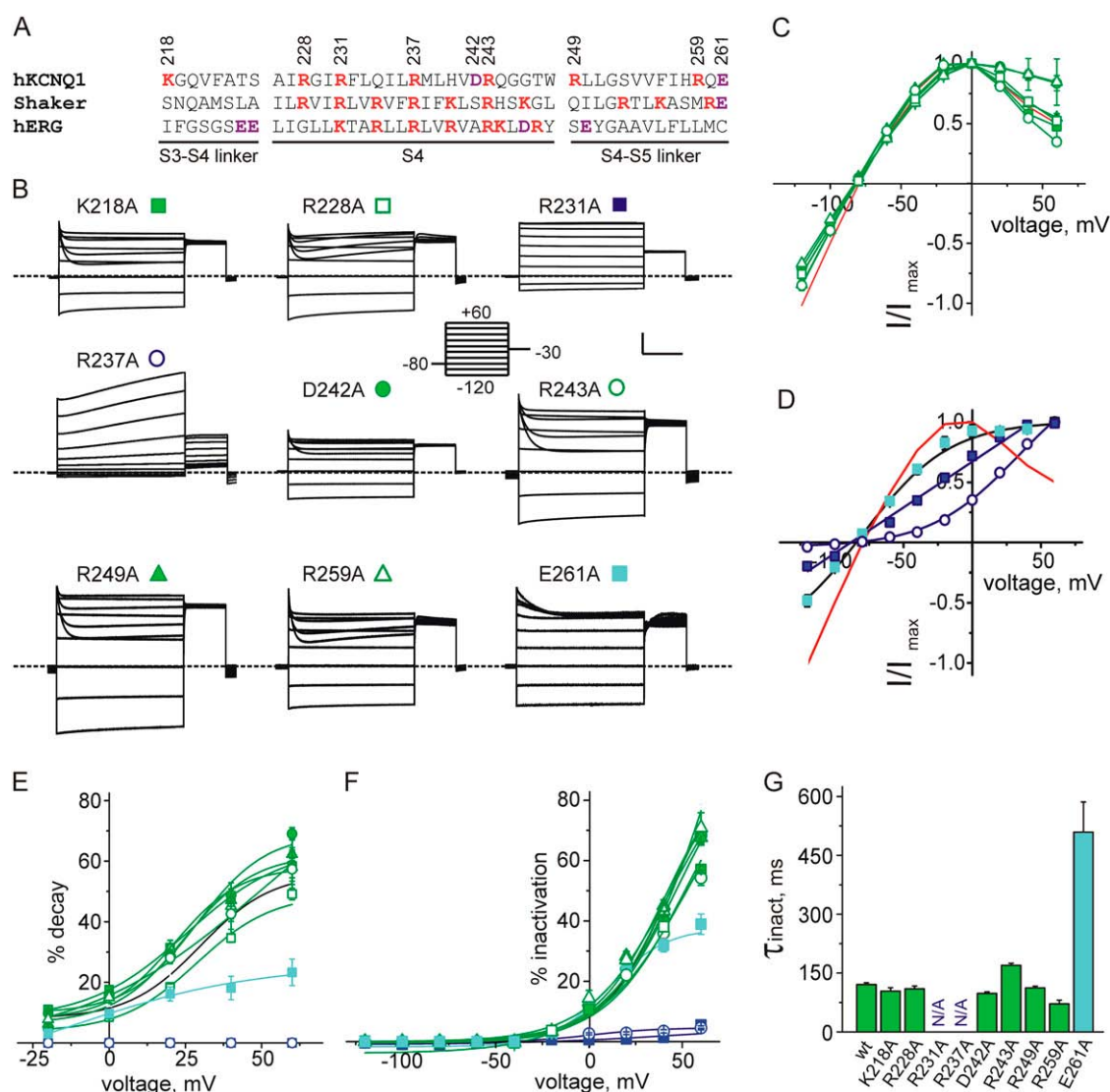
FIGURE 7 Effects of charge neutralization in S4 and surrounding linkers on F340W-I_{Ks} inactivation. (*A*) Sequence alignment for predicted S3-S4 linker, S4 and S4-S5 linker of human KCNQ1, *Shaker*, and hERG. (*Red*) Basic residues; (*purple*) acidic residues. Charged residues in KCNQ1 are numbered at top. (*B*) Exemplar traces for F340W-I_{Ks} channels with each of the charged residues highlighted in panel *A* sequentially mutated to alanine. Voltage protocol inset as in Fig. 1. (*Scale bars*) horizontal, 1 s; vertical: 1.5 μA (K218A and R228A); 1 μA (R231A and R243A); 6 μA (R237A); 0.5 μA (D242A, R249A, and R259A); and 0.2 μA (E261A). (*Dashed lines*) Zero current level. (*C*) Mean normalized *I/V* relationships for F340W-I_{Ks} channels containing K218A, R228A, D242A, R243A, R249A, or R259A mutation, symbols as in panel *A*. For these and for panel *D*, current was measured at the end of the pulse, or at the nadir of the current amplitude in cases where the decay was followed by a slow, voltage-dependent activation, $n = 4$–14 oocytes per group. Error bars indicate SEM. (*Red line*) Fit for single-mutant F340W-I_{Ks} channels for comparison. (*D*) Mean normalized *I/V* relationship for F340W-I_{Ks} channels containing R231A, R237A, or E261A mutation, symbols as in panel *A*, $n = $ 9–13 oocytes per group. Error bars indicate SEM. (*Red line*) Fit for single mutant F340W-I_{Ks} channel for comparison. (*E*) Mean current decay versus voltage during test pulse for all double mutants in panel *A*, symbols as in panel *A*, $n = 4$–14 oocytes per group. Error bars indicate SEM. (*Black line*) Fit for single-mutant F340W-I_{Ks} channels for comparison. (*F*) Mean inactivation versus voltage calculated by assessing the fraction of available channels from the initial tail current after each voltage step to current after the -120 mV voltage step, for all double-mutants in panel *A*, symbols as in panel *A*, $n = 4$–14 oocytes per group. Error bars indicate SEM. (*G*) Estimation of inactivation rate expressed as τ_{inact} for F340W-I_{Ks} (*wt*) and all double-mutants from panel *A*, derived from a single-exponential fit of current decay for purposes of direct comparison, $n = 4$–14 oocytes per group. Error bars indicate SEM. *N/A*, not applicable (no visible, time-dependent current decay).

Effects of R231A and R237A mutations in F340W-KCNQ1 versus F340W-I_{Ks} channels

To exclude the possibility that the R231A and R237A mutations simply prevented interaction with MinK, we compared currents with/without MinK coexpression. MinK increased R231A,F340W-KCNQ1 current density ~10-fold,

thus coassembly was preserved; both currents showed essentially linear *I/V* relationship and no time-dependent current decay between -120 and $+40$ mV (Fig. 8, *A* and *B*). MinK increased R237A,F340W-KCNQ1 current approximately fivefold at $+40$ mV and removed the current decay and inward rectification observed for homomeric R237A,F340W-
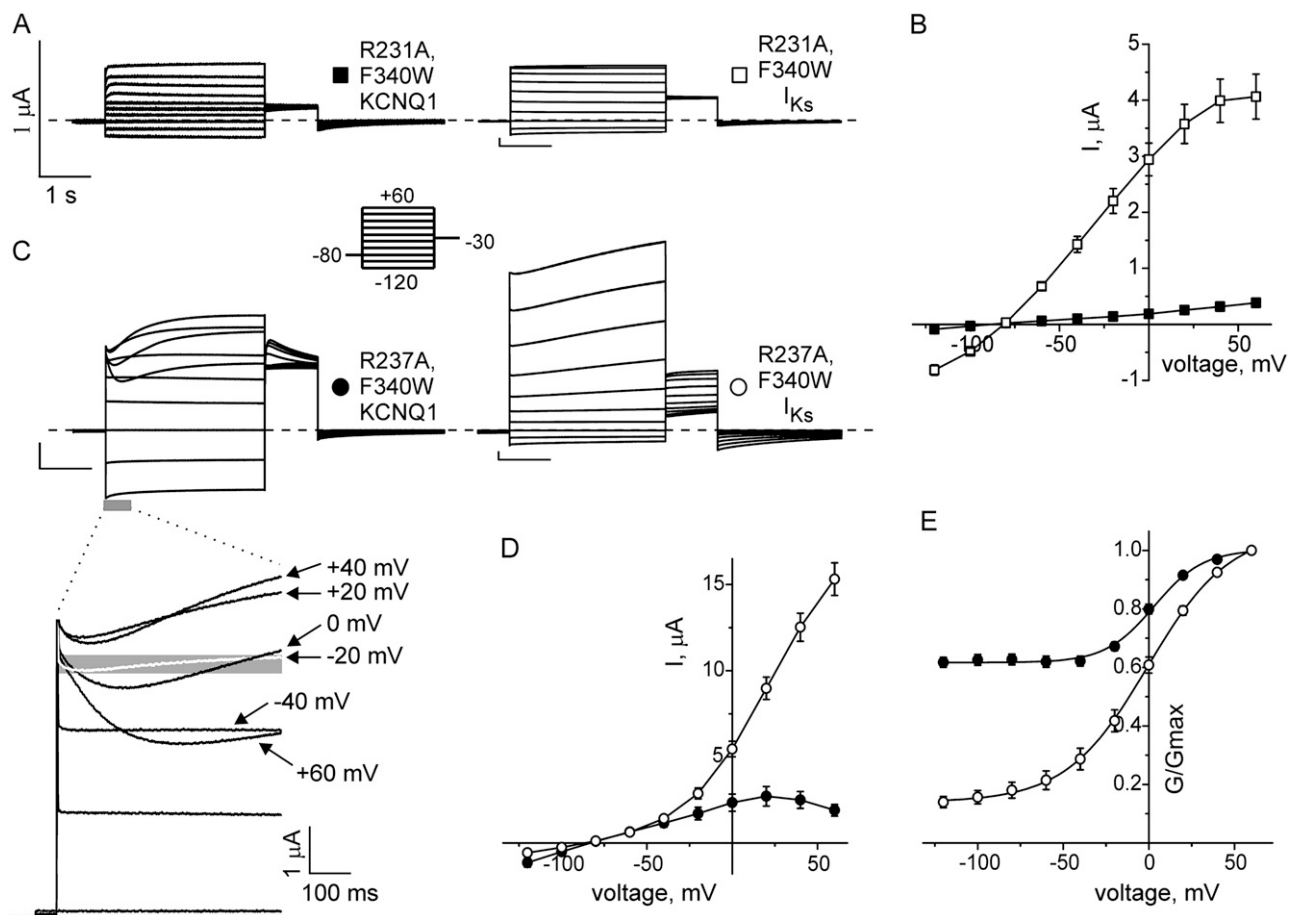
FIGURE 8 Effects of MinK in F340W-I$_{Ks}$ channels bearing R231A or R237A S4 mutations. (*A*) Exemplar traces for R231A,F340W-KCNQ1 and R231A,F340W-I$_{Ks}$ channels as indicated. Voltage protocol inset as in Fig. 7. (*Scale bars*) Horizontal, 1 s; and vertical, 1 μA. (*Dashed lines*) Zero current level. (*B*) Mean raw *I/V* relationship for R231A,F340W-KCNQ1 and R231A,F340W-I$_{Ks}$ channels, symbols as in panel *A*, *n* = 12–13 oocytes per group. Error bars indicate SEM. (*C*) Exemplar traces for R237A,F340W-KCNQ1 and R237A,F340W-I$_{Ks}$ channels as indicated. Voltage protocol as for panel *A*. (*Scale bars*) Horizontal, 1 s; and vertical, 1 μA. (*Dashed lines*) Zero current level. (*Lower left inset*) First 500 ms of R237A,F340W-KCNQ1 traces showing similar voltage dependence of activation and inactivation, first evident at −20 mV (*open trace, shaded background*). (*Dashed line*) Zero current level, scale bar for inset as shown. (*D*) Mean raw *I/V* relationship for R237A,F340W-KCNQ1 and R237A,F340W-I$_{Ks}$ channels, symbols as in panel *C*, *n* = 8–10 oocytes per group. Error bars indicate SEM. (*E*) Mean normalized *G/V* relationship from tail current for R237A,F340W-KCNQ1 and R237A,F340W-I$_{Ks}$ channels, symbols as in panel *C*, *n* = 8–10 oocytes per group. Error bars indicate SEM. Data were fit with a Boltzmann function. R237A,F340W-KCNQ1: A_1, 0.62 ± 0.01; A_2, 1.0 ± 0.01; $V_{1/2}$, 3.1 ± 2.0 mV; and V_s, 14.2 ± 1.6 mV. R237A,F340W-I$_{Ks}$: A_1, 0.14± 0.01; A_2, 1.07 ± 0.02; $V_{1/2}$, −0.64 ± 2.0 mV; and V_s, 23.8 ± 0.2 mV.

KCNQ1 channels, which exhibited voltage-dependent activation and inactivation (Fig. 8, *C* and *D*). These processes exhibited similar voltage dependence, as apparent from the appearance of current decay and of time-dependent activation at similar voltages (Fig. 8 *C*, inset). Further, while MinK removed inactivation of R237A,F340W-KCNQ1 channels (assessed as loss of both current decay and inward rectification), it did not alter the voltage-dependence of activation (assessed from normalized *G/V* relationships), although the fraction of constitutive current was reduced (Fig. 8 *E*). These data are consistent with a gating scheme in which the voltage dependence of activation and inactivation arises from a similar entity (i.e., S4) and in which the two gating processes are separable. Furthermore, the faster kinetics of inactivation versus activation (Fig. 8 *C*) is more consistent with two parallel processes

than with a scheme in which inactivation follows activation in series.

R231A,F340W-I$_{Ks}$ channels exhibit constitutive inactivation

The absence of current decay in R231A,F340W-I$_{Ks}$ channels posed the question of whether C-type inactivation was absent, or occurring constitutively and in a voltage-independent fashion. Previously, we found that I$_{Ks}$ channels with the R231A mutation but not the F340W mutation exhibit constitutive activation but no inactivation (60). These data indicated that in otherwise wild-type I$_{Ks}$, the R231A mutation results in S4 activation even at hyperpolarized potentials. Here, we assessed the existence of constitutive, voltage-

dependent C-type inactivation in R231A,F340W-I_{Ks} channels by examining the effects of different extracellular monovalent cations (as in Fig. 4). R231A,F340W-I_{Ks} channels exhibited no visible current decay during the 3 s test pulse, regardless of voltage or ion species (Fig. 9, A–D). Increasing the concentration of extracellular permeant ions, using either 100 mM K^+ or Rb^+, increased the outward current at positive voltages compared to the 4 K^+/96 Na^+ extracellular solution despite a decrease in driving force (Fig. 9, B and C).
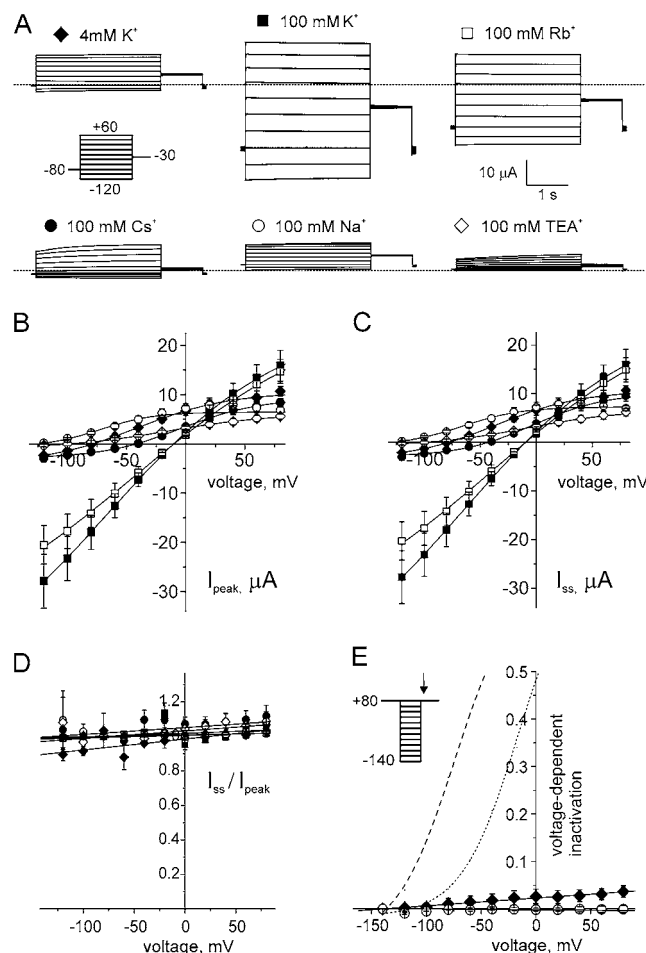
FIGURE 9 Effect of external permeant ions on R231A,F340W-I_{Ks} currents. (A) Exemplar current traces recorded in oocytes expressing R231A,F340W-I_{Ks} channels using the protocol inset. Bath solution was varied such that the monovalent cations comprised 4 mM K^+/96 mM Na^+, or 100 mM K^+, Rb^+, Cs^+, Na^+, or TEA^+ as indicated. (Dashed lines) Zero current levels. (B) Raw peak I/V relationships for oocytes as in panel A, n = 10–12. Symbols as in panel A. Error bars indicate SEM. (C) Raw steady-state I/V relationships (end of 3-s test pulse) from oocytes as in panel A, n = 10–12. Symbols as in panel A. Error bars indicate SEM. (D) Steady-state current as a fraction of peak current for recordings as in panels B and C, symbols as in panel A, n = 10–12. Error bars indicate SEM. (E) Voltage-dependence of inactivation assessed using the partial recovery protocol inset (arrow indicates where currents are measured) for R231A,F340W-I_{Ks} channels with 4 K^+/96 Na^+ (solid diamonds) or 100 mM Na^+ (open circles) bath solution, indicating little or no voltage-dependent inactivation. Boltzmann fits for similar analysis of F340W-I_{Ks} channels with 4 K^+/96 Na^+ (dotted line) or 100 mM Na^+ (dashed line) bath solution shown for comparison.

Conversely, decreasing the concentration of permeant extracellular ions, using 100 mM Na^+, resulted in decreased current amplitude despite an increase in driving force (Fig. 9, A–C). With 100 mM extracellular TEA^+, another relatively impermeant ion, current was also decreased, although this could arise partially from weak block (56); currents with 100 mM extracellular Cs^+ also resulted in a small reduction at more positive voltages (Fig. 9, A–C), unlike for F340W-I_{Ks} (Fig. 4), explored further below. Using both the fractional decay calculation (Fig. 9 D) and the partial recovery protocol (Fig. 9 E), it was evident that little or no time and voltage-dependent inactivation was occurring during the course of the test pulses in either protocol, regardless of external ion, for R231A,F340W-I_{Ks} channels. The increase in outward current with increased extracellular permeant ion, against driving force, was therefore suggestive of a degree of constitutive C-type inactivation or similar constitutive process, which was limiting ion flux due to constriction or other conformational changes within the pore.

Increased extracellular permeant ion concentration increases outward currents in R231A,F340W-I_{Ks} but not R231A-I_{Ks} channels

To further test the hypothesis that increased extracellular permeant ion concentration increases outward R231A,F340W-I_{Ks} current at positive voltages because of relief from constitutive inactivation, effects of varying the external ions were also tested on single-mutant R231A-I_{Ks} channels, which exhibit constitutive activation but are thought to exhibit no inactivation, constitutive or otherwise (60). In all cases, R231A-I_{Ks} currents varied according to driving force, thus increasing permeant extracellular ion concentration (with 100 mM K^+ or Rb^+) reduced outward current amplitude relative to 4 K^+/96 Na^+ whereas current amplitude was increased with 100 mM extracellular Na^+; essentially the reverse was true for R231A,F340W-I_{Ks} channels (Fig. 10). Current amplitude with 100 mM extracellular TEA^+ was decreased relative to 4 K^+/96 Na^+ current for either channel, but to a lesser extent for R231A-I_{Ks} channels (Fig. 10). These TEA^+ data may also support the case for constitutive inactivation in R231A,F340W-I_{Ks}, although it is feasible that this effect could arise from a shift in sensitivity to block by TEA^+.

Permeability calculations suggest constitutive pore constriction in R231A,F340W-I_{Ks} channels

C-type inactivation of Kv channels such as *Shaker* is thought to constitute a conformational change or constriction in the pore, near or at the selectivity filter (11,12). Here, we exploited shifts in reversal potential with altered extracellular monovalent cations to estimate permeability ratios for F340W-I_{Ks}, R231A,F340W-I_{Ks}, and wild-type I_{Ks} channels using a modification of the GHK voltage equation (Eq. 6). F340W-I_{Ks} channels inactivate little and slowly at more
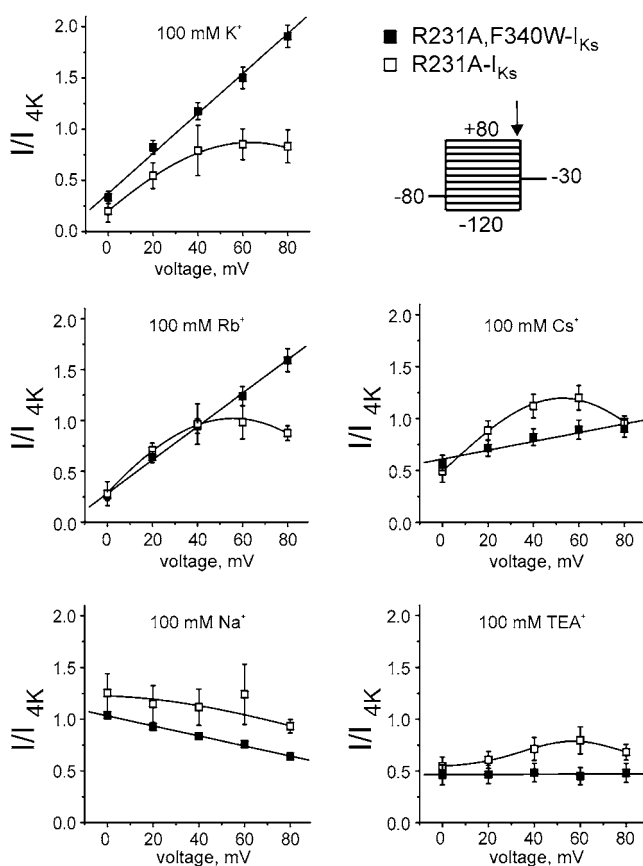
FIGURE 10 External permeant ions increase outward currents against driving force for R231A,F340W-I$_{Ks}$ but not R231A-I$_{Ks}$ channels. Late currents from R231A,F340W-I$_{Ks}$ (as in Fig. 9; *solid squares*) and R231A-I$_{Ks}$ (raw data not shown; *open squares*) channels in a range of single extracellular monovalent cations (as indicated) normalized to late current using 4 K$^+$/96 Na$^+$ bath solution, between 0 and +80 mV; $n = 4$–12. Protocol inset, (*arrow*) at which current was measured. Error bars indicate SEM.

negative potentials, thus one would expect little or no inactivation at peak current at the potentials used for calculating permeability ratios, using a standard voltage family protocol (Fig. 4). Correspondingly, the permeability series for F340W-I$_{Ks}$ favored the larger ionic radii, following the order Cs$^+$ > Rb$^+$ > K$^+$ ≫ Na$^+$ (Fig. 11, *B* and *C*), demonstrating that noninactivated F340W-I$_{Ks}$ channels are unusually permeable to Cs$^+$, suggesting a wider pore than typical K$^+$-selective channels.

Next, the same approach was used to estimate permeability ratios for F340W-I$_{Ks}$ channels at a range of voltages immediately after being held at +80 mV for 1 s to favor steady-state inactivation (Fig. 11, *A* and *B*). This was applied to assess whether the permeability ratios—and thus selectivity filter—were altered by inactivation, with two caveats: first, that the channel populations would, particularly at very negative voltages, already be entering various stages of inactivation recovery as this process occurs so rapidly upon repolarization; second, the greater the permeability of the ion used, the greater the protection from pore collapse and

therefore most likely the lesser the degree of inactivation. This aside, the permeability ratio for F340W-I$_{Ks}$ channels held at a voltage favorable to inactivation (probably an average of inactivated channels, some channels recovering from inactivation, and some protected from inactivation depending on the permeant ion) was qualitatively different from that of noninactivated F340W-I$_{Ks}$ channels, the former exhibiting a calculated permeability series of K$^+$ > Rb$^+$ > Cs$^+$ ≫ Na$^+$, suggestive of some constriction of the selectivity filter when moving to a voltage-favoring inactivation, disfavoring Cs$^+$ movement through the inactivated pore (Fig. 11 *C*). The mean permeability of F340W-I$_{Ks}$ for Cs$^+$ relative to K$^+$ dropped from 1.23 ± 0.09 to 0.77 ± 0.13 ($n = 8$–12; $p < 0.05$)—a 38% reduction when using the voltage protocol favoring inactivation (Fig. 11 *C*). Interestingly, the relative permeability for Na$^+$ increased using the +80 mV prepulse to favor inactivation (*open squares*, Fig. 11 *C*) compared to when measured at the peak current with a standard voltage family protocol (*open circles*, Fig. 11 *C*). This shift may also reflect pore constriction, to an extent that Na$^+$ permeability is favored, in the inactivated state.

A qualitatively similar but more prominent trend against Cs$^+$ conduction compared to that of K$^+$ was calculated for R231A,F340W-I$_{Ks}$ channels (K$^+$ > Rb$^+$ ≫ Cs$^+$ > Na$^+$) suggestive of a constitutive constriction of the selectivity filter, favoring K$^+$ over larger ions (Fig. 11, *B* and *C*; from currents as in Fig. 9). The R231A mutation reduced the relative Cs$^+$ permeability (compared to K$^+$) of F340W-I$_{Ks}$ channels from 1.23 ± 0.09 to 0.24 ± 0.02 ($n = 9$–12; $p < 0.0001$)—an 80% reduction—(Fig. 11 *C*). This, as with the data in Figs. 9 and 10, was consistent with both the hypothesis that a significant proportion of R231A,F340W-I$_{Ks}$ channels are in a constitutively C-type inactivated state with a pore configuration more permissive to K$^+$ flux than Cs$^+$ flux, and the hypothesis that this inactivation involves a qualitatively similar constriction of the selectivity filter to that occurring during the voltage-dependent inactivation observed here for F340W-I$_{Ks}$ channels. Again, it should be noted that because more permeant ions probably protect from inactivation by disfavoring pore collapse, greater relative conduction of a given ion is likely due to both the pore size/configuration favoring its permeation, and this in turn disfavoring to some extent inactivation. Finally, using the same protocol as in Fig. 11 *A* to ensure open channels even at negative voltages, wild-type I$_{Ks}$ channels—which exhibit voltage-dependent activation but do not inactivate—were found to exhibit a more standard permeability ratio expected for a K$^+$-selective channel (K$^+$ ≫ Rb$^+$ ≫ Cs$^+$ > Na$^+$), suggesting that the F340W mutation perturbs the pore such that, compared to wild-type I$_{Ks}$ channels, the selectivity filter of F340W-I$_{Ks}$ channels is relatively permissive to Cs$^+$ when in the open, noninactivated state. The Cs$^+$ permeability relative to K$^+$ permeability for wild-type I$_{Ks}$ was calculated to be 0.18 ± 0.05 ($n = 10$; not significantly different from that of R231A,F340W; Fig. 11, *B* and *C*).
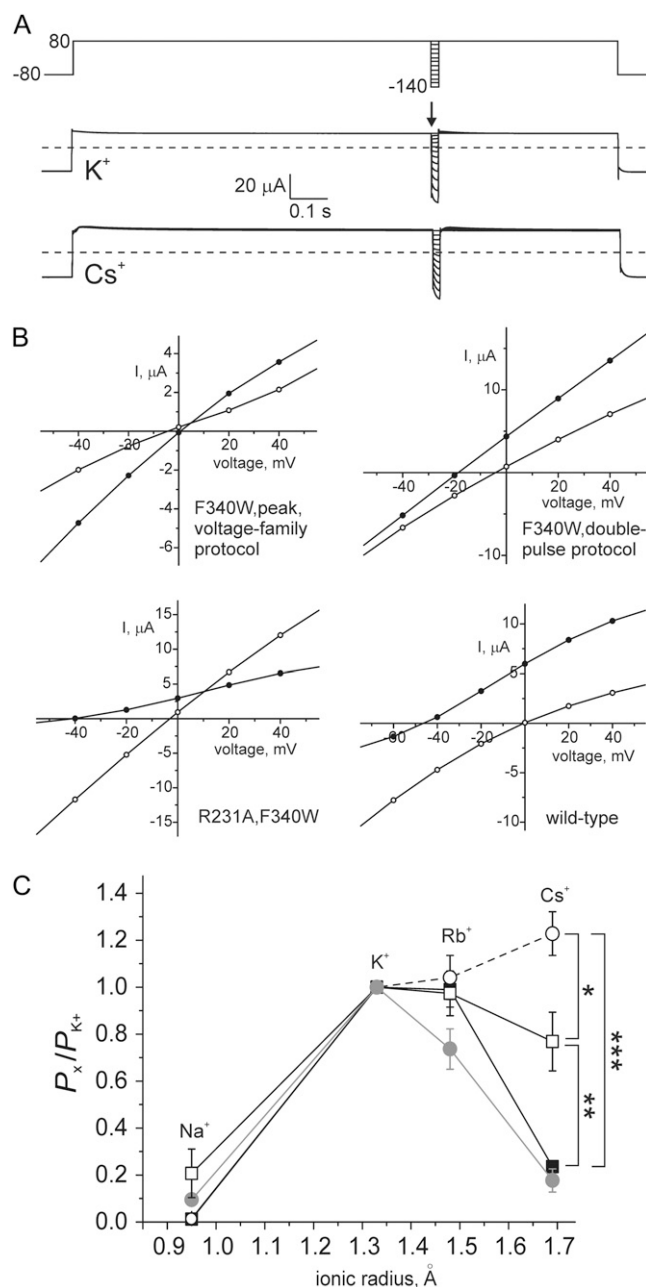
FIGURE 11 Permeability series of F340W-I_{Ks} and R231A,F340W-I_{Ks} channels. (*A*) (*Upper*) Partial recovery protocol incorporating a 1 s pulse to +80 mV followed by a 20-ms inactivation recovery step to voltages between −140 and +80 mV, then a 500-ms +80 mV tail pulse. (*Lower*) Exemplar traces recorded in oocytes expressing F340W-I_{Ks} with 100 mM K^+ or Cs^+ bath solution as indicated, using protocol above. Measurement at the arrow permits assessment of current at a range of voltages with minimal inactivation recovery after preinactivation at 80 mV. (*Dashed line*) Zero current level. (*B*) Exemplar *I/V* relationships for individual oocytes expressing I_{Ks} variants as indicated with 100 mM K^+ (*open circles*) or Cs^+ (*solid circles*) bath solution. For measurement of wild-type channels, and F340W channels to favor inactivation, the protocol in panel *A* was used, and current measured at the arrow. For R231A,F340W and noninactivated F340W channels, the voltage family protocol as in Fig. 9 *A* was employed, and current measured at the start of the test pulse. (*C*) Estimated mean permeability relative to that of K^+ versus ionic radius (Pauling) for Na^+, Rb^+, and Cs^+ through F340W-I_{Ks} (voltage-family protocol peak current, *open circles*; panel *A* protocol,

DISCUSSION

KCNQ1 is somewhat unique among Kv channel α-subunits, even when compared to the other four known KCNQ subunits. KCNQ1 is expressed ubiquitously around the body including the heart, GI tract, inner ear, and a range of secretory epithelia but not the central nervous system; in contrast, the other KCNQ subunits are almost exclusively expressed in the central nervous system (63). Homomeric KCNQ1 channels undergo an unusual form of slow inactivation which is weakly voltage-sensitive and not affected by extracellular monovalent cation species (33). The other KCNQ channels also exhibit voltage-dependent inactivation, although this has only recently been studied quantitatively (64). KCNQ1 has the lowest net S4 charge (+3) of any known eukaryotic voltage-gated cation channel, with two fewer basic residues than any of the other KCNQ subunits (26,60). KCNQ1 is modulated by all of the five known KCNE ancillary subunits (MiRPs) with varying effects (31), and so far all its known roles in physiology require association with KCNE subunits: MinK (KCNE1) in the heart and inner ear (29,30); MiRP1 (KCNE2) in parietal cells (65–68); and probably MiRP2 (KCNE3) in colonic epithelium (65,69). KCNQ1 is the only voltage-gated ion channel to be converted to a constitutively active (voltage-independent) channel by association with ancillary subunits (MiRP1 and MiRP2), now known to require the prior-mentioned KCNQ1 S4 charge paucity (60). KCNQ1 is thus a specialized yet highly adaptable α-subunit due to variable functional modulation by ancillary subunits. Understanding its normal gating processes, and the impact on these processes of mutagenesis or modulation by ancillary subunits, will permit drawing of parallels with better understood channels such as *Shaker*, elucidate how the unique features of KCNQ1 permit its functional flexibility in heteromeric complexes, and ultimately direct design of drugs to modulate its function to avert pathophysiological dysfunction of this channel in the context of any or all of its various diverse physiological guises.

F340—a hub for KCNQ1 gating

Kv channels open when the membrane is depolarized and most commonly also undergo a slow inactivation process during prolonged membrane depolarization. This slow in-

open squares), R231A,F340W-I_{Ks} (*solid squares*) and wild-type I_{Ks} (*shaded circles*) channels. Relative permeability was calculated based on shifts in reversal potential with varying 100 mM external ion solutions for individual oocytes as in panel *B* (recordings as in Figs. 4 *A*, 9 *A*, and 11 *A*; $n = 8$–12) using a variant of the GHK voltage equation (Eq. 6). Error bars indicate SEM. Statistical significance for comparison of relative permeability of Cs^+: *$p < 0.05$; **$p < 0.01$; and ***$p < 0.0001$. Values for relative permeability ratios, in the order Na^+, Rb^+, and Cs^+: F340W-I_{Ks} voltage-family protocol peak current, 0.01, 1.04, and 1.23; F340W-I_{Ks} panel *A* protocol, 0.21, 0.97, and 0.77; R231A,F340W-I_{Ks}, 0.01, 0.99, and 0.24; and wild-type I_{Ks}, 0.10, 0.74, and 0.18.

activation, termed C-type in most cases, is believed to involve constriction in both the outer and inner mouths of the channel pore, thus preventing ion permeation (70–72). Previously, specific substitutions (alanine or glycine, but not isoleucine or leucine) at V310, predicted to be at the base of the pore helix in KCNQ1, were found to dramatically increase inactivation of homomeric KCNQ1 channels, and also introduce a constitutive component to KCNQ1 activation (although activation was still largely time- and voltage-dependent) (73). In that report, it was suggested that the side chain of residue 310 interacts with residues within the S5 and S6 domains, and it was found that mutation of F340 also increased both constitutive current and inactivation of homomeric KCNQ1—tryptophan was not tested, but isoleucine introduced the largest constitutive component of those substitutions tested.

F340 is crucial for control of KCNQ1 gating by MinK, via interaction with T58 in the transmembrane domain of MinK (41–43). In homomeric KCNQ1 channels the F340W mutation not only induces a component of constitutive activation, it also increases the extent of inactivation. Further, the F340W mutation alters the effects of MinK on KCNQ1 on both activation and inactivation: MinK increases inactivation and constitutive activation of F340W-KCNQ1, whereas MinK removes inactivation and positively shifts and slows activation of wild-type KCNQ1 (34). In sum, these data underscore the remarkable functional flexibility of KCNQ1 and suggest that F340 is, in effect, a hub for cross talk between the activation and inactivation gates of KCNQ1 and also for modulation of these gates by MinK and potentially other MiRPs. Indicative of the sensitivity of this hub, the relatively subtle substitution of phenylalanine for tryptophan at position 340 essentially uncouples activation from voltage and introduces a form of inactivation with C-type properties and intrinsic voltage dependence.

KCNQ1 S6 and constitutive activation

A previous study of the mechanism of constitutive activation of a mutant *Shaker* potassium channel offers some parallels with results obtained from analyses of the F340W-I$_{Ks}$ channel. A P475D mutation in *Shaker* S6 resulted in constitutive activation with relatively large macroscopic conductance even at -150 mV (74). Results from that study suggested that the constitutive conductance of P475D resulted from perturbation of the open-closed state equilibrium that destabilized the closed state irrespective of voltage, and without the necessity for S4 voltage-sensor movement. KCNQ1-F340 aligns with *Shaker* I470, situated between *Shaker* P475 (in the putative activation-gate region) and the postulated glycine hinge (*Shaker* G466) (Fig. 1). KCNQ1 does not harbor the highly-conserved glycine hinge residue (instead, it is an alanine) and thus flexibility at this position is not thought to be important for KCNQ1 gating (73). Despite this, the closely-positioned (at least in primary structure) KCNQ1

F340W and *Shaker* P475D mutations both result in constitutive activation. This is consistent with analogous activation mechanisms for the two channels with respect to the role of S6, suggesting that similar destabilization of the closed state occurs with both KCNQ1-F340W and *Shaker*-P475D and also that KCNQ1, like *Shaker*, undergoes a voltage-independent step during activation. This tallies with previous reports that KCNQ1 exhibits at least two open states (and two closed states), with the C_2-O_1 transition being almost voltage-independent (33) and the rate-limiting step in wild-type I$_{Ks}$ channels (75).

Lu et al. (61) suggested a four-step gating scheme for *Shaker* channels in which the two closed states (C_{S4} and C^{S4}) are separated by a voltage-dependent step (θK_S), which represents S4 movement, as are the two open states: O_{S4} and O^{S4}, separated by K_S (Fig. 12 A). The C_{S4}-O_{S4} and C^{S4}-O^{S4} transitions are voltage-independent and are separated by equilibrium constants θK_G and K_G, respectively. Voltage-dependence of activation is proposed to stem from inequality between the latter constants such that K_G is much larger than θK_G. P475D-*Shaker* channels are suggested to have the ability to open either before or after depolarization-initiated S4 movement because the balance between the K_G and θK_G equilibrium constants has shifted dramatically (61,74). In the case of F340W-I$_{Ks}$, a similar shift in balance caused by the F340W mutation could favor the observed channel opening without S4 activation; subsequent depolarization appears to activate S4 but in this case the only gate linked in any tangible form to S4 status is the C-type inactivation gate, which is probably formed by residues in or around the selectivity filter (Figs. 7 and 8).

Voltage-dependent inactivation in a constitutively open channel

F340W-I$_{Ks}$ inactivation bears hallmarks of C-type—instantaneous onset upon depolarization and sensitivity to extracellular permeant cations. These features, and also the activation-independent voltage dependence of inactivation, were rendered amenable to direct quantification because of the constitutive activation of F340W-I$_{Ks}$ channels. Wild-type I$_{Ks}$ channels do not exhibit inactivation at all, suggesting that the inactivation gate in I$_{Ks}$ channels is stable in the open state regardless of voltage.

Previously, Pusch et al. (75) demonstrated that wild-type, homomeric KCNQ1 (but not I$_{Ks}$) channels exhibit voltage-dependent block by intracellular Na$^+$ ions in the absence of extracellular K$^+$, with 65 mM intracellular Na$^+$ and K$^+$. While this block also manifested as time-dependent decay at depolarized voltages, several pieces of evidence suggest against block by intracellular Na$^+$ ions (Na$_i^+$) as the mechanism for decay of F340W-I$_{Ks}$ currents. First, in a constitutively active channel, one would not expect block by a small ion to cause current decay over hundreds of milliseconds, but rather to produce inward rectification because of submillisecond block kinetics without measurable time-dependent
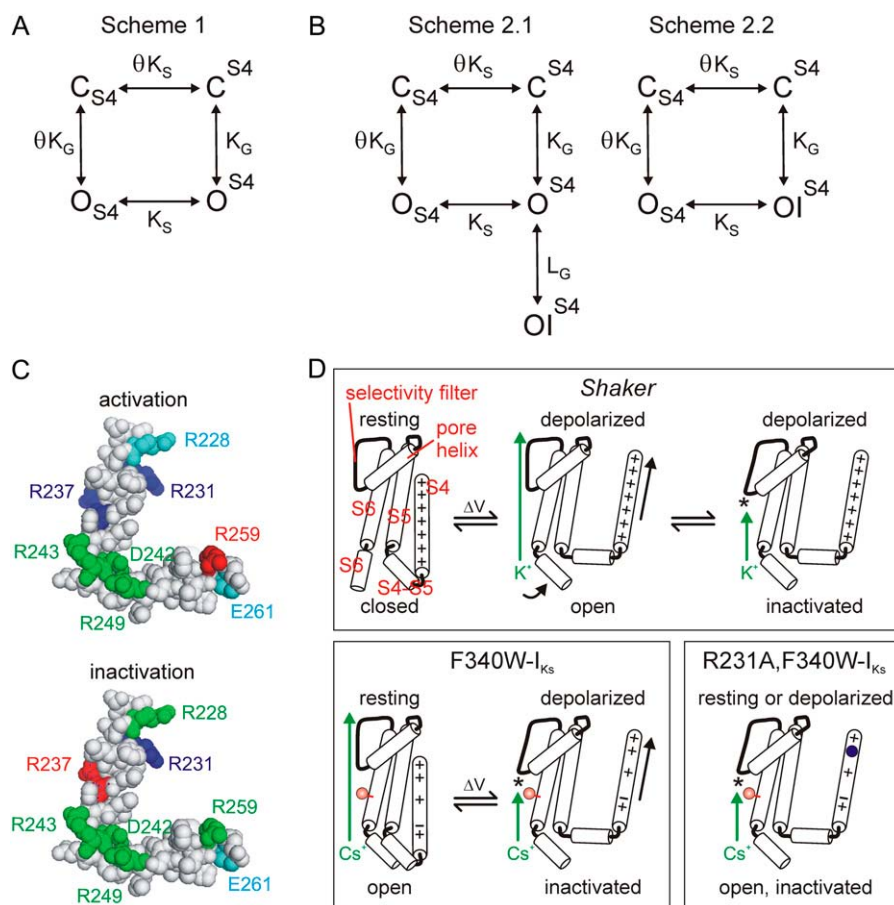
FIGURE 12 Impact of S4 and S6 mutations on C-type inactivation in I_{Ks}. (*A*) Minimal four-step gating scheme proposed for *Shaker* (61,62). (*B*) Modifications of minimal four-step gating scheme proposed as possible schemes for F340W-I_{Ks}. Symbols, *O*, open; *C*, closed, *I*, inactivated; and S4 position indicated by subscript for down-position and superscript for up-position. Equilibrium constants *K* and *L* are discussed in the text. (*C*) Space-filling models of KCNQ1 S4 and S4-S5 linker (see Methods) with charged residues color-coded to relative effects of the less positive charge in each position on activation (*upper*) or inactivation (*lower*). (*Dark blue*, increased constitutive activation or inactivation; *light blue*, increased/speeded activation or inactivation; *red*, reduced constitutive activation or inactivation; and *green*, no significant effect.) (*D*) Proposed activation/inactivation gating models for *Shaker*, F340W-I_{Ks}, and R231A,F340W-I_{Ks} as indicated. (*Red sphere*) F340W mutation; (*blue sphere*) R231A mutation; (*asterisk*) C-type inactivated state; domains are labeled in red in upper-left cartoon and apply to all; conduction pathway indicated by green arrow in each case; proposed movement of domains indicated by black arrows.

decay, as also observed in Kv channels other than KCNQ1 (76). Block of wild-type KCNQ1 is thought to be uniquely slow because there are two open states, the latter one being relatively more sensitive to block by Na_i^+ (75). Second, one would not expect S4 charge neutralizations to eliminate the time-dependent portion of this block, as we observe for R231A,F340W-I_{Ks}. Third, wild-type I_{Ks} block by Na_i^+ is not time-dependent but instantaneous, unlike homomeric KCNQ1. Fourth, block by Na_i^+ is generally relieved at higher depolarizing voltages whereas F340W-I_{Ks} current decay is not (at least up to +100 mV). Fifth, significant block by Na_i^+ is typically only observed with highly elevated Na_i^+ (75,76).

C-type inactivation in other channels (e.g., *Shaker*, Kv2.1) is not considered to exhibit voltage-dependence independent of the voltage-dependence of channel opening, but it is thought that depolarization-initiated S4 motion alters the conformation of S6 to open the channel, disrupting interaction of S6 with the edge of the pore and destabilizing the open state of the inactivation gate, leading to C-type inactivation (19,77). In a model constructed to explain C-, P-, and U-type inactivation in *Shaker*, Kv2.1, and Kv3.1 channels, the development of C- and P-type inactivation is described as "essentially voltage-independent" (78).

Our data demonstrate that C-type inactivation can develop in the absence of the microscopic C-O activation step. The

data also demonstrate that the S4-derived voltage-dependence of the S6 shift that constitutes activation in typical voltage-activated K^+ channels is not required for the C-type inactivation to be voltage-dependent; in F340W-I_{Ks} channels, inactivation retains its voltage-dependence even when the F340W S6 mutation has locked open the activation gate, rendering it essentially voltage-independent between −140 mV and +80 mV. The voltage-dependence of F340W-I_{Ks} inactivation is not, therefore, merely a knock-on effect of voltage-dependent S6 movement. It could, however, involve perturbation of S6 by the F340W mutation such that inactivation gate closure is favored once S4 is switched to the on-conformation by depolarization, analogous to the allosteric model for speeding of C-type inactivation by N-type inactivation proposed by Rasmusson et al. (79), in which binding of the inactivation domain within the pore is proposed to induce a conformational change in S6 that favors inactivation gate closure.

We contend that the voltage-dependent inactivation observed in F340W-I_{Ks} channels and the constitutive inactivation observed in R231A,F340W-I_{Ks} channels reflect the same process except that, in the latter case, the R231A substitution is a surrogate for membrane depolarization, favoring the on-conformation of S4 even at hyperpolarized potentials. The evidence for this contention is threefold: the two processes

involve similar pore constriction as evidenced from qualitatively similar permeability series; elevated concentrations of external permeant ions increase current against driving force in either case; and—specifically arguing for the role of S4—while in one case (F340W) inactivation is voltage-dependent, in the other case (R231A,F340W) the voltage dependence is lost by introducing the same mutation (R231A) that we previously found to ablate voltage dependence of activation in otherwise wild-type I$_{Ks}$ channels (60).

Two possible minimal gating schemes related to that previously proposed for *Shaker* (61) (Fig. 12 *A*) are discussed here for F340W-I$_{Ks}$. In Scheme 2.1 (Fig. 12 *B*), to reach the open, inactivated state (OI^{S4}) requires a voltage-dependent transition, O$_{S4}$-O^{S4}, then a voltage-independent transition controlled by the equilibrium constant L$_G$, O^{S4}-OI^{S4}. In Scheme 2.2, the O^{S4} state is replaced by OI^{S4}, such that the inactivation itself is intrinsically voltage-dependent, i.e., O$_{S4}$-OI^{S4}. Scheme 2.1 is certainly possible from our data, as although the activation gate appears essentially locked open by the F340W mutation, there could be an undetected but rapid, voltage-dependent conformational shift in the activation gate required before entering the inactivated state. However, we favor a model incorporating intrinsically voltage-dependent inactivation, suggesting Scheme 2.2, for several reasons. First, F340W-I$_{Ks}$ inactivation occurred with essentially instantaneous onset yet strong voltage dependence upon depolarization (Fig. 2). Second, F340W-I$_{Ks}$ inactivation rate was intrinsically voltage-dependent, a feature not observed in channels that also activate voltage-dependently, as even if there were an unresolved, ultrarapid voltage-dependent activation step it would be difficult to use this to explain the voltage dependence of decay kinetics which occurred over tens to hundreds of milliseconds (Fig. 3 *B*). One could argue that if the structure of the activation gate was equivalent for the two open states in Scheme 2.1 then this transition would be undetectable and impossible to distinguish from Scheme 2.2; but if this were the case, one would also expect inactivation to occur voltage-independently from O$_{S4}$ (61,74) and we have no evidence that this occurs to any great extent with F340W-I$_{Ks}$ (although it is not absolutely precluded). Third, data acquired from the R237A,F340W mutant channels also offer evidence in support of voltage-dependent inactivation stemming directly from S4 independent of voltage-dependent opening. Homomeric R237A,F340W-KCNQ1 channels (lacking MinK) exhibit a clear time- and voltage-dependent component to opening, the voltage-dependence of which appears similar to that of the inactivation process in these channels because, we propose, both are linked to the same voltage-sensor movement (Fig. 8 *C, inset*). However, the inactivation process in these channels is clearly much faster than the voltage-dependent opening process, as if the inactivation is initiated in parallel with channel opening upon S4 movement rather than the inactivation occurring in series once opening has occurred. This would mirror hERG inactivation, which is intrinsically voltage-dependent (although

not classic C-type in nature) and much faster than hERG opening (49,80). Furthermore, introduction of MinK into the complex to form R237A,F340W-I$_{Ks}$ retained the slow, time- and voltage-dependent opening component without a significant change in $V_{1/2}$, but eliminated both the voltage-dependent inactivation (Fig. 8 *C*) and the majority of the constitutively open component (assessed from the relatively small current component at −120 mV in the test pulse and in the tail current *G/V* relationship; see Fig. 8 *E*). This is again consistent with the inactivation occurring from the constitutively open state (O$_{S4}$) rather than the voltage-dependently open state (O^{S4}).

Evidence for molecular events underlying F340W-I$_{Ks}$ inactivation

Assuming that F340W-I$_{Ks}$ inactivation is voltage-dependent and follows Scheme 2.2, we can infer the following other mechanistic aspects of inactivation in this channel:

1. The voltage dependence involves S4, because of the effects of charge neutralizations at R231 and R237 (Fig. 7).
2. The S4 conformational change that occurs in F340W-I$_{Ks}$ channels to initiate inactivation probably resembles that which occurs in wild-type I$_{Ks}$ channels to initiate activation, based on the somewhat similar positional effects of charge mutants on the voltage dependence of either process in the two channel types (Fig. 12 *C* and (60)).
3. The number of equivalent gating charges that are transferred during F340W-I$_{Ks}$ inactivation (z_i) appears to be ~1, calculated either from the voltage dependence of inactivation kinetics (Fig. 3 *B*) or from a Boltzmann fit of the extent of inactivation after reaching steady-state, then permitting a brief recovery period (Fig. 2 *C*). This could arise from a relatively subtle shift of one charge in each of the four voltage sensors partway across the membrane electric field, or alternatively could suggest that only one S4 domain needs to move in response to membrane depolarization, with a consequent crossing of a single positive charge across the entire membrane field, for the channel to inactivate—mimicking N-type inactivation in which only one of potentially four inactivation domains is required to block the conduction pathway (8). Because for F340W-I$_{Ks}$ in the 4 K$^+$/96 Na$^+$ bath solution there appears to be a rapid component to inactivation (τ_2), which is either voltage-independent or just becomes so fast at positive voltages that we cannot resolve the voltage dependence of its kinetics, one could contend that we are underestimating the z_i value. However, the calculation of z_i from the Boltzmann fit of inactivation using the partial recovery protocol was in good agreement with the estimation from linear regression of the inactivation rate constant, and the former method should account at least in part for unresolved events at higher

depolarized voltages because it evaluates extent of inactivation, not kinetics. Furthermore, previous calculations of z for wild-type I_{Ks} activation also yielded a value of 1 (47), consistent with our hypothesis that the voltage dependence of F340W-I_{Ks} inactivation and of wild-type I_{Ks} activation arises from the same charged voltage sensor, S4.

Finally, we make three further conclusions from combined data derived from estimations of relative permeability, the contra-driving force effects on outward current amplitude of extracellular permeant ions, and the effects of extracellular permeant ions on the kinetics of inactivation and inactivation recovery (Figs. 4–11):

4. F340W-I_{Ks} inactivation involves constriction of the selectivity filter/pore region.
5. Noninactivated F340W-I_{Ks} favors Cs^+ permeation over K^+ whereas C-type inactivated F340W-I_{Ks} favors K^+ permeation over Cs^+.
6. Some fraction of R231A,F340W-I_{Ks} channels are held in a largely voltage-independent, constitutively C-type inactivated OI^{S4} state, which is more permeable to K^+ than Cs^+ ions.

CONCLUSION

These suggested mechanistic distinctions are illustrated in Fig. 12 *D*. *Shaker* C-type inactivation is conceptualized as developing essentially voltage-independently in series after voltage-dependent activation: S4 senses membrane depolarization and undergoes a conformational change that is coupled to the activation gate (primarily S6) by the S4-S5 linker; after this a purportedly voltage-independent inactivation process occurs which involves constriction of the upper pore (19,77). In contrast, F340W-I_{Ks} channels are constitutively open (O_{S4} state), with the S6 activation gate independent of S4 and permissive to Cs^+ conduction at rest. Upon depolarization there is some degree of pore constriction as the channel enters the OI^{S4} state (closing of the inactivation gate), associated with a voltage- and time-dependent reduction in permeability to K^+, Rb^+, and especially Cs^+. This process is altered by mutation of S4 charged residues, suggesting involvement of S4 in the voltage-dependence of inactivation. R231A,F340W-I_{Ks} channels, because S4 activation is favored even at hyperpolarized potentials, are constitutively in an open, inactivated state (OI^{S4}), which is relatively nonpermissive to Cs^+ conduction.

F340W-I_{Ks} channels and the variants described herein demonstrate the centrality of F340 in I_{Ks} gating, the functional flexibility of the KCNQ1 channel, and the existence of voltage-dependent C-type inactivation—constituting a unique system in which further aspects of C-type inactivation can be studied without the contaminating process of voltage-dependent activation.

REFERENCES

1. Inoue, I. 1981. Activation-inactivation of potassium channels and development of the potassium-channel spike in internally perfused squid giant axons. *J. Gen. Physiol.* 78:43–61.

2. Muramatsu, I., M. Noda, M. Nishio, and M. Fujiwara. 1987. Mechanism of sodium channel block in crayfish giant axons by 711389-S, a new antiarrhythmic drug. *J. Pharmacol. Exp. Ther.* 242:269–276.

3. Baukrowitz, T., and G. Yellen. 1995. Modulation of K^+ current by frequency and external $[K^+]$: a tale of two inactivation mechanisms. *Neuron.* 15:951–960.

4. Ruppersberg, J. P., R. Frank, O. Pongs, and M. Stocker. 1991. Cloned neuronal IK_A channels reopen during recovery from inactivation. *Nature.* 353:657–660.

5. Turrigiano, G. G., E. Marder, and L. F. Abbott. 1996. Cellular short-term memory from a slow potassium conductance. *J. Neurophysiol.* 75:963–966.

6. Jow, F., Z. H. Zhang, D. C. Kopsco, K. C. Carroll, and K. Wang. 2004. Functional coupling of intracellular calcium and inactivation of voltage-gated $Kv_{1.1}/Kv_{\beta 1.1}$ A-type K^+ channels. *Proc. Natl. Acad. Sci. USA.* 101:15535–15540.

7. Lichtinghagen, R., M. Stocker, R. Wittka, G. Boheim, W. Stuhmer, A. Ferrus, and O. Pongs. 1990. Molecular basis of altered excitability in *Shaker* mutants of *Drosophila melanogaster*. *EMBO J.* 9:4399–4407.

8. Hoshi, T., W. N. Zagotta, and R. W. Aldrich. 1990. Biophysical and molecular mechanisms of *Shaker* potassium channel inactivation. *Science.* 250:533–538.

9. Murrell-Lagnado, R. D., and R. W. Aldrich. 1993. Energetics of *Shaker* K channels block by inactivation peptides. *J. Gen. Physiol.* 102:977–1003.

10. Murrell-Lagnado, R. D., and R. W. Aldrich. 1993. Interactions of amino terminal domains of *Shaker* K channels with a pore blocking site studied with synthetic peptides. *J. Gen. Physiol.* 102:949–975.

11. Hoshi, T., W. N. Zagotta, and R. W. Aldrich. 1991. Two types of inactivation in *Shaker* K^+ channels: effects of alterations in the carboxy-terminal region. *Neuron.* 7:547–556.

12. Kurata, H. T., and D. Fedida. 2006. A structural interpretation of voltage-gated potassium channel inactivation. *Prog. Biophys. Mol. Biol.* 92:185–208.

13. Fedida, D., N. D. Maruoka, and S. Lin. 1999. Modulation of slow inactivation in human cardiac $Kv_{1.5}$ channels by extra- and intracellular permeant cations. *J. Physiol.* 515:315–329.

14. Levy, D. I., and C. Deutsch. 1996. Recovery from C-type inactivation is modulated by extracellular potassium. *Biophys. J.* 70:798–805.

15. Ogielska, E. M., and R. W. Aldrich. 1999. Functional consequences of a decreased potassium affinity in a potassium channel pore. Ion interactions and C-type inactivation. *J. Gen. Physiol.* 113:347–358.

16. Eghbali, M., R. Olcese, M. M. Zarei, L. Toro, and E. Stefani. 2002. External pore collapse as an inactivation mechanism for $Kv_{4.3}$ K^+ channels. *J. Membr. Biol.* 188:73–86.

17. Gomez-Lagunas, F. 2001. Na^+ interaction with the pore of *Shaker* B K^+ channels: zero and low K^+ conditions. *J. Gen. Physiol.* 118:639–648.

18. Gomez-Lagunas, F. 1997. *Shaker* B K^+ conductance in Na^+ solutions lacking K^+ ions: a remarkably stable non-conducting state produced by membrane depolarizations. *J. Physiol.* 499:3–15.

19. Loots, E., and E. Y. Isacoff. 1998. Protein rearrangements underlying slow inactivation of the *Shaker* K^+ channel. *J. Gen. Physiol.* 112:377–389.

20. Ogielska, E. M., W. N. Zagotta, T. Hoshi, S. H. Heinemann, J. Haab, and R. W. Aldrich. 1995. Cooperative subunit interactions in C-type inactivation of K channels. *Biophys. J.* 69:2449–2457.

21. Klemic, K. G., C. C. Shieh, G. E. Kirsch, and S. W. Jones. 1998. Inactivation of Kv$_{2.1}$ potassium channels. *Biophys. J.* 74:1779–1789.

22. Olcese, R., R. Latorre, L. Toro, F. Bezanilla, and E. Stefani. 1997. Correlation between charge movement and ionic current during slow inactivation in *Shaker* K$_+$ channels. *J. Gen. Physiol.* 110:579–589.

23. Neyroud, N., F. Tesson, I. Denjoy, M. Leibovici, C. Donger, J. Barhanin, S. Faure, F. Gary, P. Coumel, C. Petit, K. Schwartz, and P. Guicheney. 1997. A novel mutation in the potassium channel gene KVLQT1 causes the Jervell and Lange-Nielsen cardioauditory syndrome. *Nat. Genet.* 15:186–189.

24. Nicolas, M., D. Dememes, A. Martin, S. Kupershmidt, and J. Barhanin. 2001. KCNQ1/KCNE1 potassium channels in mammalian vestibular dark cells. *Hear. Res.* 153:132–145.

25. Wang, Q., M. E. Curran, I. Splawski, T. C. Burn, J. M. Millholland, T. J. VanRaay, J. Shen, K. W. Timothy, G. M. Vincent, T. de Jager, P. J. Schwartz, J. A. Toubin, A. J. Moss, D. L. Atkinson, G. M. Landes, T. D. Connors, and M. T. Keating. 1996. Positional cloning of a novel potassium channel gene: KVLQT1 mutations cause cardiac arrhythmias. *Nat. Genet.* 12:17–23.

26. Yang, W. P., P. C. Levesque, W. A. Little, M. L. Conder, F. Y. Shalaby, and M. A. Blanar. 1997. KvLQT1, a voltage-gated potassium channel responsible for human cardiac arrhythmias. *Proc. Natl. Acad. Sci. USA.* 94:4017–4021.

27. Splawski, I., K. W. Timothy, G. M. Vincent, D. L. Atkinson, and M. T. Keating. 1997. Molecular basis of the long-QT syndrome associated with deafness. *N. Engl. J. Med.* 336:1562–1567.

28. Splawski, I., M. Tristani-Firouzi, M. H. Lehmann, M. C. Sanguinetti, and M. T. Keating. 1997. Mutations in the hminK gene cause long QT syndrome and suppress I$_{Ks}$ function. *Nat. Genet.* 17:338–340.

29. Barhanin, J., F. Lesage, E. Guillemare, M. Fink, M. Lazdunski, and G. Romey. 1996. K(V)LQT1 and IsK (minK) proteins associate to form the I$_{Ks}$ cardiac potassium current. *Nature.* 384:78–80.

30. Sanguinetti, M. C., M. E. Curran, A. Zou, J. Shen, P. S. Spector, D. L. Atkinson, and M. T. Keating. 1996. Coassembly of K(V)LQT1 and minK (IsK) proteins to form cardiac I$_{Ks}$ potassium channel. *Nature.* 384:80–83.

31. McCrossan, Z. A., and G. W. Abbott. 2004. The MinK-related peptides. *Neuropharmacology.* 47:787–821.

32. Seebohm, G., M. C. Sanguinetti, and M. Pusch. 2003. Tight coupling of rubidium conductance and inactivation in human KCNQ1 potassium channels. *J. Physiol.* 552:369–378.

33. Pusch, M., R. Magrassi, B. Wollnik, and F. Conti. 1998. Activation and inactivation of homomeric KvLQT1 potassium channels. *Biophys. J.* 75:785–792.

34. Tristani-Firouzi, M., and M. C. Sanguinetti. 1998. Voltage-dependent inactivation of the human K$^+$ channel KvLQT1 is eliminated by association with minimal K$^+$ channel (minK) subunits. *J. Physiol.* 510:37–45.

35. Sigworth, F. J. 2001. Potassium channel mechanics. *Neuron.* 32:555–556.

36. Jiang, Y., A. Lee, J. Chen, M. Cadene, B. T. Chait, and R. MacKinnon. 2002. The open pore conformation of potassium channels. *Nature.* 417:523–526.

37. Ding, S., L. Ingleby, C. A. Ahern, and R. Horn. 2005. Investigating the putative glycine hinge in *Shaker* potassium channel. *J. Gen. Physiol.* 126:213–226.

38. Seebohm, G., N. Strutz-Seebohm, O. N. Ureche, R. Baltaev, A. Lampert, G. Kornichuk, K. Kamiya, T. V. Wuttke, H. Lerche, M. C. Sanguinetti, and F. Lang. 2006. Differential roles of S6 domain hinges in the gating of KCNQ potassium channels. *Biophys. J.* 90:2235–2244.

39. Webster, S. M., D. Del Camino, J. P. Dekker, and G. Yellen. 2004. Intracellular gate opening in *Shaker* K+ channels defined by high-affinity metal bridges. *Nature.* 428:864–868.

40. Labro, A. J., A. L. Raes, I. Bellens, N. Ottschytsch, and D. J. Snyders. 2003. Gating of *Shaker*-type channels requires the flexibility of S6 caused by prolines. *J. Biol. Chem.* 278:50724–50731.

41. Panaghie, G., K. K. Tai, and G. W. Abbott. 2006. Interaction of KCNE subunits with the KCNQ1 K$^+$ channel pore. *J. Physiol.* 570:455–467.

42. Melman, Y. F., A. Krumerman, and T. V. McDonald. 2002. A single transmembrane site in the KCNE-encoded proteins controls the specificity of KvLQT1 channel gating. *J. Biol. Chem.* 277:25187–25194.

43. Melman, Y. F., S. Y. Um, A. Krumerman, A. Kagan, and T. V. McDonald. 2004. KCNE1 binds to the KCNQ1 pore to regulate potassium channel activity. *Neuron.* 42:927–937.

44. Yarov-Yarovoy, V., D. Baker, and W. A. Catterall. 2006. Voltage sensor conformations in the open and closed states in ROSETTA structural models of K$^+$ channels. *Proc. Natl. Acad. Sci. USA.* 103:7292–7297.

45. Schwede, T., J. Kopp, N. Guex, and M. Peitsch. 2003. SWISS-MODEL: an automated protein homology-modeling server. *Nucleic Acids Res.* 31:3381–3385.

46. Long, S. B., E. B. Campbell, and R. Mackinnon. 2005. Voltage sensor of Kv$_{1.2}$: structural basis of electromechanical coupling. *Science.* 309:903–908.

47. Sesti, F., and S. A. Goldstein. 1998. Single-channel characteristics of wild-type I$_{Ks}$ channels and channels formed with two minK mutants that cause long QT syndrome. *J. Gen. Physiol.* 112:651–663.

48. Long, S. B., E. B. Campbell, and R. Mackinnon. 2005. Crystal structure of a mammalian voltage-dependent *Shaker* family K$^+$ channel. *Science.* 309:897–903.

49. Smith, P. L., T. Baukrowitz, and G. Yellen. 1996. The inward rectification mechanism of the HERG cardiac potassium channel. *Nature.* 379:833–836.

50. Wang, Z., and D. Fedida. 2001. Gating charge immobilization caused by the transition between inactivated states in the Kv$_{1.5}$ channel. *Biophys. J.* 81:2614–2627.

51. Sanguinetti, M. C., C. Jiang, M. E. Curran, and M. T. Keating. 1995. A mechanistic link between an inherited and an acquired cardiac arrhythmia: HERG encodes the I$_{Kr}$ potassium channel. *Cell.* 81:299–307.

52. Demo, S. D., and G. Yellen. 1991. The inactivation gate of the *Shaker* K$^+$ channel behaves like an open-channel blocker. *Neuron.* 7:743–753.

53. Lopez-Barneo, J., T. Hoshi, S. H. Heinemann, and R. W. Aldrich. 1993. Effects of external cations and mutations in the pore region on C-type inactivation of *Shaker* potassium channels. *Receptors Channels.* 1:61–71.

54. Starkus, J. G., S. H. Heinemann, and M. D. Rayner. 2000. Voltage dependence of slow inactivation in *Shaker* potassium channels results from changes in relative K$^+$ and Na$^+$ permeabilities. *J. Gen. Physiol.* 115:107–122.

55. Shimizu, H., C. Toyoshima, and S. Oiki. 2003. Interaction between tetraethylammonium and permeant cations at the inactivation gate of the HERG potassium channel. *Jpn. J. Physiol.* 53:25–34.

56. Kurokawa, J., H. K. Motoike, and R. S. Kass. 2001. TEA$^+$-sensitive KCNQ1 constructs reveal pore-independent access to KCNE1 in assembled I$_{Ks}$ channels. *J. Gen. Physiol.* 117:43–52.

57. Ahern, C. A., A. L. Eastwood, H. A. Lester, D. A. Dougherty, and R. Horn. 2006. A cation-π interaction between extracellular TEA and an aromatic residue in potassium channels. *J. Gen. Physiol.* 128:649–657.

58. Andalib, P., J. F. Consiglio, J. G. Trapani, and S. J. Korn. 2004. The external TEA binding site and C-type inactivation in voltage-gated potassium channels. *Biophys. J.* 87:3148–3161.

59. Heginbotham, L., and R. MacKinnon. 1992. The aromatic binding site for tetraethylammonium ion on potassium channels. *Neuron.* 8:483–491.

60. Panaghie, G., and G. W. Abbott. 2007. The role of S4 charges in voltage-dependent and voltage-independent KCNQ1 potassium channel complexes. *J. Gen. Physiol.* 129:121–133.

61. Lu, Z., A. M. Klem, and Y. Ramu. 2002. Coupling between voltage sensors and activation gate in voltage-gated K$^+$ channels. *J. Gen. Physiol.* 120:663–676.

62. Franqueza, L., M. Lin, J. Shen, I. Splawski, M. T. Keating, and M. C. Sanguinetti. 1999. Long QT syndrome-associated mutations in the S4–S5 linker of KvLQT1 potassium channels modify gating and interaction with minK subunits. *J. Biol. Chem.* 274:21063–21070.

63. Robbins, J. 2001. KCNQ potassium channels: physiology, pathophysiology, and pharmacology. *Pharmacol. Ther.* 90:1–19.

64. Jensen, H. S., M. Grunnet, and S. P. Olesen. 2007. Inactivation as a new regulatory mechanism for neuronal Kv_7 channels. *Biophys. J.* 92:2747–2756.

65. Dedek, K., and S. Waldegger. 2001. Colocalization of KCNQ1/KCNE channel subunits in the mouse gastrointestinal tract. *Pflugers Arch.* 442:896–902.

66. Heitzmann, D., F. Grahammer, T. von Hahn, A. Schmitt-Graff, E. Romeo, R. Nitschke, U. Gerlach, H. J. Lang, F. Verrey, J. Barhanin, and R. Warth. 2004. Heteromeric KCNE2/KCNQ1 potassium channels in the luminal membrane of gastric parietal cells. *J. Physiol.* 561:547–557.

67. Lambrecht, N. W., I. Yakubov, D. Scott, and G. Sachs. 2005. Identification of the K efflux channel coupled to the gastric H-K-ATPase during acid secretion. *Physiol. Genomics.* 21:81–91.

68. Roepke, T. K., A. Anantharam, P. Kirchhoff, S. M. Busque, J. B. Young, J. P. Geibel, D. J. Lerner, and G. W. Abbott. 2006. The KCNE2 potassium channel ancillary subunit is essential for gastric acid secretion. *J. Biol. Chem.* 281:23740–23747.

69. Schroeder, B. C., S. Waldegger, S. Fehr, M. Bleich, R. Warth, R. Greger, and T. J. Jentsch. 2000. A constitutively open potassium channel formed by KCNQ1 and KCNE3. *Nature.* 403:196–199.

70. Liu, Y., M. E. Jurman, and G. Yellen. 1996. Dynamic rearrangement of the outer mouth of a K^+ channel during gating. *Neuron.* 16:859–867.

71. Castle, N. A., S. R. Fadous, D. E. Logothetis, and G. K. Wang. 1994. 4-Aminopyridine binding and slow inactivation are mutually exclusive in rat $Kv_{1.1}$ and *Shaker* potassium channels. *Mol. Pharmacol.* 46:1175–1181.

72. Li, X., G. C. Bett, X. Jiang, V. E. Bondarenko, M. J. Morales, and R. L. Rasmusson. 2003. Regulation of N- and C-type inactivation of $Kv_{1.4}$ by pH_0 and K^+: evidence for transmembrane communication. *Am. J. Physiol. Heart Circ. Physiol.* 284:H71–H80.

73. Seebohm, G., P. Westenskow, F. Lang, and M. C. Sanguinetti. 2005. Mutation of colocalized residues of the pore helix and transmembrane segments S5 and S6 disrupt deactivation and modify inactivation of KCNQ1 K^+ channels. *J. Physiol.* 563:359–368.

74. Sukhareva, M., D. H. Hackos, and K. J. Swartz. 2003. Constitutive activation of the *Shaker* Kv channel. *J. Gen. Physiol.* 122:541–556.

75. Pusch, M., L. Ferrera, and T. Friedrich. 2001. Two open states and rate-limiting gating steps revealed by intracellular Na^+ block of human KCNQ1 and KCNQ1/KCNE1 K^+ channels. *J. Physiol.* 533:135–143.

76. Bezanilla, F., and C. M. Armstrong. 1972. Negative conductance caused by entry of sodium and cesium ions into the potassium channels of squid axons. *J. Gen. Physiol.* 60:588–608.

77. Loots, E., and E. Y. Isacoff. 2000. Molecular coupling of S4 to a K^+ channel's slow inactivation gate. *J. Gen. Physiol.* 116:623–636.

78. Klemic, K. G., G. E. Kirsch, and S. W. Jones. 2001. U-type inactivation of $Kv_{3.1}$ and *Shaker* potassium channels. *Biophys. J.* 81:814–826.

79. Rasmusson, R. L., M. J. Morales, S. Wang, S. Liu, D. L. Campbell, M. V. Brahmajothi, and H. C. Strauss. 1998. Inactivation of voltage-gated cardiac K^+ channels. *Circ. Res.* 82:739–750.

80. Zhang, M., J. Liu, and G. N. Tseng. 2004. Gating charges in the activation and inactivation processes of the HERG channel. *J. Gen. Physiol.* 124:703–718.